A Study of Quantum Error Correction by Geometric Algebra and Liquid-State NMR Spectroscopy

Y. Sharf and D. G. Cory
Dept. of Nuclear Engineering
Massachusetts Institute of Technology
Cambridge, MA 02139

S. S. Somaroo and T. F. Havel*
BCMP, Harvard Medical School
240 Longwood Ave., Boston, MA 02115

E. Knill (CIC-3), R. Laflamme
and W. H. Zurek (T-6)
Los Alamos National Laboratory
Los Alamos, NM 87545

April 11, 2000

*To whom correspondence should be addressed.

Abstract

Quantum error correcting codes enable the information contained in a quantum state to be protected from decoherence due to external perturbations. Applied to NMR, quantum coding does not alter normal relaxation, but rather converts the state of a "data" spin into multiple quantum coherences involving additional *ancilla* spins. These multiple quantum coherences relax at differing rates, thus permitting the original state of the data to be approximately reconstructed by mixing them together in an appropriate fashion. This paper describes the operation of a simple, three-bit quantum code in the product operator formalism, and uses geometric algebra methods to obtain the error-corrected decay curve in the presence of arbitrary correlations in the external random fields. These predictions are confirmed in both the totally correlated and uncorrelated cases by liquid-state NMR experiments on ^{13}C-labeled alanine, using gradient-diffusion methods to implement these idealized decoherence models. Quantum error correction in weakly polarized systems requires that the ancilla spins be prepared in a *pseudo-pure* state relative to the data spin, which entails a loss of signal that exceeds any potential gain through error correction. Nevertheless, this study shows that quantum coding can be used to validate theoretical decoherence mechanisms, and to provide detailed information on correlations in the underlying NMR relaxation dynamics.

1 Introduction

A quantum computer stores binary information in an array of two-state quantum systems, e.g. spin $\frac{1}{2}$ nuclei. It performs logical operations on this information via unitary transformations obtained by controlling the effective interactions among the systems. By operating on a coherent superposition over all combinations of states of the individual systems, it can, in effect, operate on all these combinations at once. This yields a degree of parallelism which grows exponentially with the size of the problem. Because such superpositions are extremely sensitive to decoherence, it was initially doubted that they could be maintained long enough to perform significant computations. Shor [**?**] and Steane [**?**] were nonetheless able to devise error correcting codes to control decoherence in quantum computers. It has now been shown that arbitrarily long quantum computations can be carried out providing the error rate per operation is below some threshold [**?**, **?**, **?**, **?**].

Even though a true quantum computer has yet to be built, small quantum computations can be performed using standard liquid-state NMR spectroscopy to operate on the nuclear spins in ensembles of molecules in pseudo-pure states [**?**, **?**]. These states may be characterized as having a density matrix with only a single nondegenerate eigenvalue, whose corresponding eigenvector transforms identically to the state vector of a true pure state. This approach has enabled all the basic operations of quantum computing to be demonstrated [**?**, **?**], including simple quantum algorithms [**?**, **?**, **?**], teleportation [**?**], and error correction [**?**]. The preparation of pseudo-pure states from equilibrium states nevertheless entails a rapid loss in signal with increasing numbers of spins [**?**, **?**, **?**], precluding the use of liquid-state NMR as a means of performing large-scale quantum computations.

This paper builds on the authors' earlier implementation of a three-bit quantum error correcting code [**?**], and consists of two parts, one theoretical and the other experimental. In the first part, geometric algebra methods [**?**] are used to derive the error corrected decay curve assuming arbitrary correlations in the relaxation processes responsible. The second describes a complete NMR implementation of the code, and demonstrates that it performs as predicted by the theory using gradient diffusion methods to implement both totally correlated

and uncorrelated T_2 relaxation. The theoretical (sections **3** – **5**) and experimental (sections **7** – **9**) parts of the paper may be read largely independently of each other. Section **2** provides an overview of the three-bit quantum error correcting code, while section **6** discusses the significance of the theory in the context of NMR. Together, the results of this paper show how quantum coding can be used not only to correct for decoherence, but also to design experiments to test specific hypotheses on the underlying relaxation mechanisms.

2 The Quantum Error Correcting Code

The theory of quantum error correcting codes, though only a few years old [**?**, **?**], is already a well-established and highly developed subject [**?**, **?**, **?**, **?**]. The "majority logic" code demonstrated in this paper protects information encoded in the joint state of three spins against arbitrary spin flip errors. Given a data spin (throughout this paper, the first) in some arbitrary state $\alpha|0\rangle + \beta|1\rangle$ (where $|0\rangle$ is the "down" (ground) state of the spin, $|1\rangle$ the "up" state, and $|\alpha|^2 + |\beta|^2 = 1$), two ancilla spins in their ground state are added to the system, obtaining $(\alpha|0\rangle + \beta|1\rangle)|00\rangle$. A unitary transformation is then applied to the system consisting of two "c-NOT" (controlled-NOT) gates conditional on the data spin (see Fig. 1). This step, called encoding, produces the state $\alpha|000\rangle + \beta|111\rangle$.

Note that rotating a spin by π in this state is the same as interchanging a pair of corresponding bits between $|000\rangle$ and $|111\rangle$, and results in an orthogonal state. Thus one can determine if a single spin flip has occured, and which spin it happened to, by a measurement that reveals which of the orthogonal subspaces $\alpha|100\rangle + \beta|011\rangle$, $\alpha|010\rangle + \beta|101\rangle$, $\alpha|001\rangle + \beta|110\rangle$ (if any) the system has moved into. If no error occured, this measurement leaves the state of the system intact, and otherwise one knows which spin needs to be rotated by π in order to fix the error. This illustrates the basic idea behind all quantum error correcting codes: the correctable errors map the subspace of valid states onto mutually orthogonal subspaces, in each of which the unitary operation needed to fix the error is known. Because these entangled subspaces cannot be measured directly, the state must be decoded so that

the error syndrome is contained in the ancillae alone. This is done with the same unitary transformation as encoding, since it is its own inverse.

In practice, the spins are subject to numerous small random perturbations from the environment arising, for example, from fluctuating external random fields, rather than single spin flips as above. Throughout this paper, these fields will be assumed to be about the x-axis in the rotating frame [**?**]. To the extent that these perturbations affect multiple spins, the data spin will lose coherence in the yz-plane despite error correction. It nevertheless follows from the linearity of quantum mechanics that the code will still prevent decoherence to first order in time, as will now be shown.

The interaction of such fields with the y and z-components of the spins has the Hamiltonian

$$\mathbf{H}_{\mathsf{x}} \;=\; \gamma^1 B^1_{\mathsf{x}}(t)\mathbf{I}^1_{\mathsf{x}} + \gamma^2 B^2_{\mathsf{x}}(t)\mathbf{I}^2_{\mathsf{x}} + \gamma^3 B^3_{\mathsf{x}}(t)\mathbf{I}^3_{\mathsf{x}}\;, \tag{1}$$

where B^k_{x} denotes the x-component of the fluctuating magnetic field at each spin, γ^k is its gyromagnetic ratio, and $\mathbf{I}^k_{\mathsf{x}} \equiv \frac{1}{2}\boldsymbol{\sigma}^k_{\mathsf{x}}$ are the usual angular momentum operators in units of $\hbar$ ($k = 1, 2, 3$). The corresponding propagator has the form $\exp(-\boldsymbol{\imath}(\chi^1\mathbf{I}^1_{\mathsf{x}} + \chi^2\mathbf{I}^2_{\mathsf{x}} + \chi^3\mathbf{I}^3_{\mathsf{x}}))$, where $\boldsymbol{\imath}$ denotes the imaginary unit and $\chi^k = \gamma^k \int_0^t B^k_{\mathsf{x}}(\tau)\mathrm{d}\tau$. In the limit of short decoherence times and hence small accumulated phase errors χ^k, a first-order expansion of this propagator is adequate, namely:

$$\exp\left(-\boldsymbol{\imath}(\chi^1\mathbf{I}^1_{\mathsf{x}} + \chi^2\mathbf{I}^2_{\mathsf{x}} + \chi^3\mathbf{I}^3_{\mathsf{x}})\right) \;\approx\; 1 - \boldsymbol{\imath}\chi^1\mathbf{I}^1_{\mathsf{x}} - \boldsymbol{\imath}\chi^2\mathbf{I}^2_{\mathsf{x}} - \boldsymbol{\imath}\chi^3\mathbf{I}^3_{\mathsf{x}} \tag{2}$$

Thus to first order this random propagator maps the encoded state to

$$\begin{aligned} (\alpha|000\rangle + \beta|111\rangle) \;&-\; \tfrac{\boldsymbol{\imath}}{2}\chi^1(\alpha|100\rangle + \beta|011\rangle) \\ &-\; \tfrac{\boldsymbol{\imath}}{2}\chi^2(\alpha|010\rangle + \beta|101\rangle) \\ &-\; \tfrac{\boldsymbol{\imath}}{2}\chi^3(\alpha|001\rangle + \beta|110\rangle)\;. \end{aligned} \tag{3}$$

The decoding operation maps this to

$$\begin{aligned}(\alpha|0\rangle+\beta|1\rangle)|00\rangle &- \tfrac{\imath}{2}\chi^1(\alpha|1\rangle+\beta|0\rangle)|11\rangle \\ &- \tfrac{\imath}{2}\chi^2(\alpha|0\rangle+\beta|1\rangle)|10\rangle \\ &- \tfrac{\imath}{2}\chi^3(\alpha|0\rangle+\beta|1\rangle)|01\rangle\ .\end{aligned} \tag{4}$$

Finally, a Toffoli gate (also called a "c^2-NOT") corrects the error, by flipping the data spin in the term in which both ancillae are "down" ($|11\rangle$). This returns the data spin to its original state $\alpha|0\rangle+\beta|1\rangle$ in that term, and otherwise leaves it alone.

Thus, in addition to single spin flips, the code corrects to first order for random, time-dependent rotations about the x-axis as claimed. By inserting a $\pi/2$ y-rotation of all the spins after encoding and its inverse before decoding, this code can be transformed to one that protects against random z-rotations, which give rise to adiabatic T_2 relaxation in NMR [**?**]. Because the code does *not* protect the ancillae, they must be "discarded" after correction, which corresponds to taking the partial trace over them. In NMR spectroscopy, this operation is performed by *decoupling* the ancillae from the data during acquisition. Note also that, since strong measurements are not available in ensembles, it is not possible to reset and reuse the ancillae for repeated error correction (see section **6** for further discussion of this issue).

The following three sections will present a detailed theoretical analysis of the code in the product operator notation of NMR [**?**, **?**], using geometric algebra methods [**?**] to compute the results of the encoding, decoherence, decoding and correction operations. Readers who are interested primarily in the experimental procedures and results should proceed directly to the main theoretical result, Eq. (43), and continue reading from there.

3 Geometric Algebra Analysis of Encoding

In NMR spectroscopy, one does not observe individual spin systems, but rather averages over macroscopic ensembles of such systems. In the semi-classical treatment of liquid-state

NMR relaxation processes used here [**?**], two distinct types of averages must be taken. The first is an average over the initial state of a typical molecule, which results, for example, in the equilibrium state $\mathbf{I}_z^1 + \mathbf{I}_z^2 + \mathbf{I}_z^3$. The second is an average over the environment of a typical molecule, or more precisely, the external random fields which act upon it. Provided the random fields are uncorrelated with the initial state, these two averages can be taken separately. In order to focus on how the results of error correction are averaged over the environment, in the following three sections it will be assumed that the spin system is initially in a pure state; the effect of averaging over an ensemble of spin systems in different pure states is considered in an Appendix.

Even though an initial pure state is assumed, the random fields from the environment will cause the state to decohere into a general mixed state, which must be described by a density matrix. The physical meaning of a density matrix is most clearly expressed using the product operator formalism, since it is based on a complete system of observables [**?**, **?**, **?**]. In the algebra generated by the product operators, spinors (pure states) correspond to *idempotents*, namely elements that are equal to their squares. In particular, spinors of the form $|\delta^1\delta^2\delta^3\rangle$ ($\delta^k = 0, 1$; $k = 1, 2, 3$) correspond to products of three idempotents, namely:

$$\mathbf{E}_\pm^1\mathbf{E}_\pm^2\mathbf{E}_\pm^3 \;\equiv\; \tfrac{1}{2}(1 + (-1)^{\delta^1} 2\mathbf{I}_z^1)\tfrac{1}{2}(1 + (-1)^{\delta^2} 2\mathbf{I}_z^2)\tfrac{1}{2}(1 + (-1)^{\delta^3} 2\mathbf{I}_z^3) \;\longleftrightarrow\; |\delta^1\delta^2\delta^3\rangle\langle\delta^1\delta^2\delta^3| \quad (5)$$

(Note that throughout this paper the scalar identity 1 is identified with the 3-spin identity operator $\mathbf{1}_8$.) Letting $\tilde{\alpha}, \tilde{\beta}$ be the complex conjugates of $\alpha, \beta \in \mathcal{C}$, and $\Re$, $\Im$ denote the real and imaginary parts, the density matrix of the data spin #1 in a general superposition state $\alpha|0\rangle + \beta|1\rangle$ is:

$$\begin{aligned}
\boldsymbol{\rho}_{\mathsf{A}}^1 &\equiv (\alpha|0\rangle + \beta|1\rangle)(\tilde{\alpha}\langle 0| + \tilde{\beta}\langle 1|) \\
&= \tfrac{1}{2}(|\alpha|^2 + |\beta|^2)(|0\rangle\langle 0| + |1\rangle\langle 1|) + \Re(\tilde{\alpha}\beta)(|1\rangle\langle 0| + |0\rangle\langle 1|) + \\
&\quad \boldsymbol{\imath}\Im(\tilde{\alpha}\beta)(|1\rangle\langle 0| - |0\rangle\langle 1|) + \tfrac{1}{2}(|\alpha|^2 - |\beta|^2)(|0\rangle\langle 0| - |1\rangle\langle 1|) \qquad (6) \\
&= \tfrac{1}{2}(|\alpha|^2 + |\beta|^2) + \Re(\tilde{\alpha}\beta)\, 2\mathbf{I}_{\mathsf{x}}^1 + \Im(\tilde{\alpha}\beta)\, 2\mathbf{I}_{\mathsf{y}}^1 + (|\alpha|^2 - |\beta|^2)\, \mathbf{I}_{\mathsf{z}}^1 \\
&= (\alpha + 2\beta\mathbf{I}_{\mathsf{x}}^1)\mathbf{E}_+^1(\tilde{\alpha} + 2\tilde{\beta}\mathbf{I}_{\mathsf{x}}^1)
\end{aligned}$$

Alternatively, an arbitrary state can be obtained by rotation of the $|0\rangle\langle 0| \equiv \mathbf{E}^1_+$ state, which may be specified in terms of polar angles as

$$\begin{aligned}
\boldsymbol{\rho}^1_{\mathsf{A}} &\equiv e^{-\boldsymbol{\iota}\phi\mathbf{I}^1_{\mathsf{z}}} e^{-\boldsymbol{\iota}\theta\mathbf{I}^1_{\mathsf{x}}} \mathbf{E}^1_+ e^{\boldsymbol{\iota}\theta\mathbf{I}^1_{\mathsf{x}}} e^{\boldsymbol{\iota}\phi\mathbf{I}^1_{\mathsf{z}}} \\
&= e^{-\boldsymbol{\iota}\phi\mathbf{I}^1_{\mathsf{z}}} (\cos(\tfrac{\theta}{2}) - 2\boldsymbol{\iota}\sin(\tfrac{\theta}{2})\mathbf{I}^1_{\mathsf{x}}) \mathbf{E}^1_+ (\cos(\tfrac{\theta}{2}) + 2\boldsymbol{\iota}\sin(\tfrac{\theta}{2})\mathbf{I}^1_{\mathsf{x}}) e^{\boldsymbol{\iota}\phi\mathbf{I}^1_{\mathsf{z}}} \\
&= (\cos(\tfrac{\theta}{2}) e^{-\boldsymbol{\iota}\phi\mathbf{I}^1_{\mathsf{z}}} - 2\boldsymbol{\iota}\sin(\tfrac{\theta}{2})\mathbf{I}^1_{\mathsf{x}} e^{\boldsymbol{\iota}\phi\mathbf{I}^1_{\mathsf{z}}}) \mathbf{E}^1_+ (e^{\boldsymbol{\iota}\phi\mathbf{I}^1_{\mathsf{z}}} \cos(\tfrac{\theta}{2}) + e^{-\boldsymbol{\iota}\phi\mathbf{I}^1_{\mathsf{z}}} 2\boldsymbol{\iota}\sin(\tfrac{\theta}{2})\mathbf{I}^1_{\mathsf{x}}) \\
&= (\cos(\tfrac{\theta}{2}) e^{-\boldsymbol{\iota}\phi/2} - 2\boldsymbol{\iota}\sin(\tfrac{\theta}{2})\mathbf{I}^1_{\mathsf{x}} e^{\boldsymbol{\iota}\phi/2}) \mathbf{E}^1_+ (e^{\boldsymbol{\iota}\phi/2} \cos(\tfrac{\theta}{2}) + e^{-\boldsymbol{\iota}\phi/2} 2\boldsymbol{\iota}\sin(\tfrac{\theta}{2})\mathbf{I}^1_{\mathsf{x}}) \ ,
\end{aligned} \tag{7}$$

where the last line was obtained by using the relation $\mathbf{I}^1_{\mathsf{z}}\mathbf{E}^1_\pm = \pm\frac{1}{2}\mathbf{E}^1_\pm$ to absorb the $\mathbf{I}^1_{\mathsf{z}}$ operators in the exponentials. A comparison of these two expressions for $\boldsymbol{\rho}^1_{\mathsf{A}}$ shows the coefficients in the superposition may be interpreted geometrically as

$$\alpha \equiv \cos(\tfrac{\theta}{2})\, e^{-\boldsymbol{\iota}\phi/2} \ , \qquad \beta \equiv -\boldsymbol{\iota}\sin(\tfrac{\theta}{2})\, e^{\boldsymbol{\iota}\phi/2} \ . \tag{8}$$

This correspondence between states and operators, which is the basis of the product operator formalism, has been used together with reformulations of multiparticle quantum mechanics in the language of geometric algebra [**?**, **?**, **?**, **?**] to obtain algebraic expressions and geometric interpretations for the basic operations of quantum computing [**?**]. Of particular interest is the fact that the propagators of c-NOT gates can also be written in terms of idempotents. Thus the particular c-NOT gate that flips the second spin when the first is "up" has the form:

$$\begin{aligned}
\mathbf{S}^{2|1} &\equiv \exp(\boldsymbol{\iota}\pi\mathbf{E}^1_-(1-2\mathbf{I}^2_{\mathsf{x}})/2) = \mathbf{E}^1_- \exp(\boldsymbol{\iota}\pi(1-2\mathbf{I}^2_{\mathsf{x}})/2) + (1-\mathbf{E}^1_-) \\
&= 2\mathbf{I}^2_{\mathsf{x}}\mathbf{E}^1_- + \mathbf{E}^1_+ = 1 - \mathbf{E}^1_-(1-2\mathbf{I}^2_{\mathsf{x}})
\end{aligned} \tag{9}$$

Using the relations $4\mathbf{I}^2_{\mathsf{x}}\mathbf{I}^2_{\mathsf{x}} = 1$, $\mathbf{I}^2_{\mathsf{x}}\mathbf{E}^2_+ = \mathbf{E}^2_-\mathbf{I}^2_{\mathsf{x}}$ and $\mathbf{E}^1_+\mathbf{E}^1_- = \mathbf{E}^1_-\mathbf{E}^1_+ = 0$, $\mathbf{S}^{2|1}$ may be shown to exchange $\mathbf{E}^2_+$ with $\mathbf{E}^2_-$ in those products containing $\mathbf{E}^1_-$; for example:

$$\begin{aligned}
\mathbf{S}^{2|1}(\mathbf{E}^1_-\mathbf{E}^2_+)\mathbf{S}^{2|1} &= (2\mathbf{I}^2_{\mathsf{x}}\mathbf{E}^1_-)(\mathbf{E}^1_-\mathbf{E}^2_+)(\mathbf{E}^1_- 2\mathbf{I}^2_{\mathsf{x}}) + \mathbf{E}^1_+(\mathbf{E}^1_-\mathbf{E}^1_+)\mathbf{E}^1_+ \\
&= \mathbf{E}^1_-(2\mathbf{I}^2_{\mathsf{x}}\tfrac{1}{2}(1+2\mathbf{I}^2_{\mathsf{z}})\, 2\mathbf{I}^2_{\mathsf{x}}) \\
&= \mathbf{E}^1_-\tfrac{1}{2}(1-8\mathbf{I}^2_{\mathsf{z}}\mathbf{I}^2_{\mathsf{x}}\mathbf{I}^2_{\mathsf{x}}) = \mathbf{E}^1_-\mathbf{E}^2_-
\end{aligned} \tag{10}$$

In a similar fashion, it can be shown that the Toffoli gate, which flips the first spin only if the other two are "up", has the form:

$$\begin{aligned} \mathbf{T}^{1|23} &\equiv \exp(\boldsymbol{\iota}\pi(1-2\mathbf{I}_{\mathsf{x}}^1)\mathbf{E}_-^2\mathbf{E}_-^3) \\ &= 2\mathbf{I}_{\mathsf{x}}^1\mathbf{E}_-^2\mathbf{E}_-^3 + (1-\mathbf{E}_-^2\mathbf{E}_-^3) \;=\; 1-(1-2\mathbf{I}_{\mathsf{x}}^1)\mathbf{E}_-^2\mathbf{E}_-^3 \end{aligned} \tag{11}$$

These are all the gates that are needed to implement the error correction procedure studied in this paper, whose operation will now be analyzed using geometric algebra.

The first step of the procedure is to encode the state $\boldsymbol{\rho}_{\mathsf{A}}^1$ of the first spin by correlating it with the ancillae in the state $\mathbf{E}_+^2\mathbf{E}_+^3$. This is done by applying the c-NOT's $\mathbf{S}^{2|1}$ and $\mathbf{S}^{3|1}$, as shown in Fig. 1. These c-NOT's commute, and their product is

$$\begin{aligned} \mathbf{S}^{2|1}\mathbf{S}^{3|1} &= (2\mathbf{I}_{\mathsf{x}}^2\mathbf{E}_-^1 + \mathbf{E}_+^1)(2\mathbf{I}_{\mathsf{x}}^3\mathbf{E}_-^1 + \mathbf{E}_+^1) \\ &= 4\mathbf{I}_{\mathsf{x}}^2\mathbf{I}_{\mathsf{x}}^3\mathbf{E}_-^1 + \mathbf{E}_+^1 \;\equiv\; \mathbf{S}^{23|1}\ . \end{aligned} \tag{12}$$

It follows that

$$\begin{aligned} \mathbf{S}^{23|1}2\mathbf{I}_{\mathsf{x}}^1\mathbf{S}^{23|1} &= (4\mathbf{I}_{\mathsf{x}}^2\mathbf{I}_{\mathsf{x}}^3\mathbf{E}_-^1 + \mathbf{E}_+^1)(2\mathbf{I}_{\mathsf{x}}^1)(4\mathbf{I}_{\mathsf{x}}^2\mathbf{I}_{\mathsf{x}}^3\mathbf{E}_-^1 + \mathbf{E}_+^1) \\ &= (2\mathbf{I}_{\mathsf{x}}^1)(4\mathbf{I}_{\mathsf{x}}^2\mathbf{I}_{\mathsf{x}}^3\mathbf{E}_+^1 + \mathbf{E}_-^1)(4\mathbf{I}_{\mathsf{x}}^2\mathbf{I}_{\mathsf{x}}^3\mathbf{E}_-^1 + \mathbf{E}_+^1) \\ &= (2\mathbf{I}_{\mathsf{x}}^1)(4\mathbf{I}_{\mathsf{x}}^2\mathbf{I}_{\mathsf{x}}^3(\mathbf{E}_+^1 + \mathbf{E}_-^1)) \;=\; 8\mathbf{I}_{\mathsf{x}}^1\mathbf{I}_{\mathsf{x}}^2\mathbf{I}_{\mathsf{x}}^3\ . \end{aligned} \tag{13}$$

Since $\mathbf{S}^{23|1}\mathbf{S}^{23|1} = 1$ and $\mathbf{S}^{23|1}$ commutes with $\mathbf{E}_+^1\mathbf{E}_+^2\mathbf{E}_+^3$, the density matrix $\boldsymbol{\rho}_{\mathsf{B}}$ of the encoded state, which is obtained by applying $\mathbf{S}^{23|1}$ to the initial density matrix $\boldsymbol{\rho}_{\mathsf{A}} \equiv \boldsymbol{\rho}_{\mathsf{A}}^1\mathbf{E}_+^2\mathbf{E}_+^3$, is given by

$$\begin{aligned} \boldsymbol{\rho}_{\mathsf{B}} &\equiv \mathbf{S}^{23|1}\boldsymbol{\rho}_{\mathsf{A}}\mathbf{S}^{23|1} \\ &= \mathbf{S}^{23|1}(\alpha + \beta 2\mathbf{I}_{\mathsf{x}}^1)\,\mathbf{S}^{23|1}\mathbf{S}^{23|1}(\mathbf{E}_+^1\mathbf{E}_+^2\mathbf{E}_+^3)\mathbf{S}^{23|1}\mathbf{S}^{23|1}(\tilde{\alpha} + \tilde{\beta}2\mathbf{I}_{\mathsf{x}}^1)\,\mathbf{S}^{23|1} \\ &= (\alpha + \beta 8\mathbf{I}_{\mathsf{x}}^1\mathbf{I}_{\mathsf{x}}^2\mathbf{I}_{\mathsf{x}}^3)(\mathbf{E}_+^1\mathbf{E}_+^2\mathbf{E}_+^3)(\tilde{\alpha} + \tilde{\beta}8\mathbf{I}_{\mathsf{x}}^1\mathbf{I}_{\mathsf{x}}^2\mathbf{I}_{\mathsf{x}}^3)\ . \end{aligned} \tag{14}$$

The product of all three $\mathbf{I}_{\mathsf{x}}$ operators in this expression reflects the entanglement of the three spins in the encoded state.

4 Averaging Over the Environment

The next step is to apply a random rotation about the x-axis to the encoded state, and then to compute the average of the result. Fortunately, the x-rotation commutes with the outer factors of $\boldsymbol{\rho}_{\mathsf{B}}$, so that it can be applied directly to the inner factor:

$$\begin{aligned} & e^{-\boldsymbol{\iota}(\chi^1\mathbf{I}_{\mathsf{x}}^1+\chi^2\mathbf{I}_{\mathsf{x}}^2+\chi^3\mathbf{I}_{\mathsf{x}}^3)}\boldsymbol{\rho}_{\mathsf{B}}e^{\boldsymbol{\iota}(\chi^1\mathbf{I}_{\mathsf{x}}^1+\chi^2\mathbf{I}_{\mathsf{x}}^2+\chi^3\mathbf{I}_{\mathsf{x}}^3)} \qquad (15) \\ = \quad & (\alpha+\beta 8\mathbf{I}_{\mathsf{x}}^1\mathbf{I}_{\mathsf{x}}^2\mathbf{I}_{\mathsf{x}}^3)e^{-\boldsymbol{\iota}(\chi^1\mathbf{I}_{\mathsf{x}}^1+\chi^2\mathbf{I}_{\mathsf{x}}^2+\chi^3\mathbf{I}_{\mathsf{x}}^3)}(\mathbf{E}_+^1\mathbf{E}_+^2\mathbf{E}_+^3)e^{\boldsymbol{\iota}(\chi^1\mathbf{I}_{\mathsf{x}}^1+\chi^2\mathbf{I}_{\mathsf{x}}^2+\chi^3\mathbf{I}_{\mathsf{x}}^3)}(\tilde{\alpha}+\tilde{\beta}8\mathbf{I}_{\mathsf{x}}^1\mathbf{I}_{\mathsf{x}}^2\mathbf{I}_{\mathsf{x}}^3) \end{aligned}$$

Since the outer factors are constant, they can be taken out of the ensemble average. This reduces the analysis of the decoherence process for arbitrary α and β to the special case in which $\alpha = 1$ and $\beta = 0$.

To facilitate this process, rewrite the inner transformation as

$$\begin{aligned} & \left(e^{-\boldsymbol{\iota}\chi^1\mathbf{I}_{\mathsf{x}}^1}\mathbf{E}_+^1e^{\boldsymbol{\iota}\chi^1\mathbf{I}_{\mathsf{x}}^1}\right)\left(e^{-\boldsymbol{\iota}\chi^2\mathbf{I}_{\mathsf{x}}^2}\mathbf{E}_+^2e^{\boldsymbol{\iota}\chi^2\mathbf{I}_{\mathsf{x}}^2}\right)\left(e^{-\boldsymbol{\iota}\chi^3\mathbf{I}_{\mathsf{x}}^3}\mathbf{E}_+^3e^{\boldsymbol{\iota}\chi^3\mathbf{I}_{\mathsf{x}}^3}\right) \\ = \quad & \tfrac{1}{8}\left(1+e^{-\boldsymbol{\iota}\chi^1\mathbf{I}_{\mathsf{x}}^1}2\mathbf{I}_{\mathsf{z}}^1e^{\boldsymbol{\iota}\chi^1\mathbf{I}_{\mathsf{x}}^1}\right)\left(1+e^{-\boldsymbol{\iota}\chi^2\mathbf{I}_{\mathsf{x}}^2}2\mathbf{I}_{\mathsf{z}}^2e^{\boldsymbol{\iota}\chi^2\mathbf{I}_{\mathsf{x}}^2}\right)\left(1+e^{-\boldsymbol{\iota}\chi^3\mathbf{I}_{\mathsf{x}}^3}2\mathbf{I}_{\mathsf{z}}^3e^{\boldsymbol{\iota}\chi^3\mathbf{I}_{\mathsf{x}}^3}\right) \qquad (16) \\ = \quad & \tfrac{1}{8}\left(1+e^{-2\boldsymbol{\iota}\chi^1\mathbf{I}_{\mathsf{x}}^1}2\mathbf{I}_{\mathsf{z}}^1\right)\left(1+e^{-2\boldsymbol{\iota}\chi^2\mathbf{I}_{\mathsf{x}}^2}2\mathbf{I}_{\mathsf{z}}^2\right)\left(1+e^{-2\boldsymbol{\iota}\chi^3\mathbf{I}_{\mathsf{x}}^3}2\mathbf{I}_{\mathsf{z}}^3\right)\ . \end{aligned}$$

Expanding this product yields the sum of all possible terms of the form

$$\mathbf{R}_{\delta^1\delta^2\delta^3}(\chi^1,\chi^2,\chi^3)\left((1-\delta^1)+\delta^1 2\mathbf{I}_{\mathsf{z}}^1\right)\left((1-\delta^2)+\delta^2 2\mathbf{I}_{\mathsf{z}}^2\right)\left((1-\delta^3)+\delta^3 2\mathbf{I}_{\mathsf{z}}^3\right) \qquad (17)$$

where

$$\mathbf{R}_{\delta^1\delta^2\delta^3}(\chi^1,\chi^2,\chi^3) \ \equiv \ e^{-2\boldsymbol{\iota}(\delta^1\chi^1\mathbf{I}_{\mathsf{x}}^1+\delta^2\chi^2\mathbf{I}_{\mathsf{x}}^2+\delta^3\chi^3\mathbf{I}_{\mathsf{x}}^3)} \qquad (18)$$

for $\delta^1,\delta^2,\delta^3 \in \{0,1\}$.

It follows that the average state can be obtained by applying the averages of the propagators $\overline{\mathbf{R}_{\delta^1\delta^2\delta^3}(\chi^1,\chi^2,\chi^3)}$ to the corresponding terms of the encoded state $\boldsymbol{\rho}_{\mathsf{B}}$. Assuming that the spectral density of the random fields $B_{\mathsf{x}}(t)$ is well-approximated by a delta-function (i.e., that the correlation time is small compared to the inverse square root of the variance in the frequencies $\gamma B_{\mathsf{x}}(t)$; see [**?**] for details), the joint probability density function of the random

angles χ^1, χ^2, χ^3 will be a multivariate Gaussian whose covariance matrix grows linearly in time. Letting $\boldsymbol{\chi} \equiv [\chi^1, \chi^2, \chi^3]^\top$ and $[\overline{\chi^k(t)\chi^\ell(t)}] \equiv [c^{jk}t] = \mathbf{C}\,t$ be the covariance matrix, this can be written as

$$P(\boldsymbol{\chi}) \;=\; \left((2\pi)^3\,\det(\mathbf{C}\,t)\right)^{-\frac{1}{2}} e^{-\frac{1}{2t}\boldsymbol{\chi}^\top \mathbf{C}^{-1}\boldsymbol{\chi}}\;. \tag{19}$$

At this point it turns out to be easier to rotate $\mathbf{R}_{\delta^1\delta^2\delta^3}(\chi^1, \chi^2, \chi^3)$ to the z-axis:

$$\begin{aligned}\mathbf{R}'_{\delta^1\delta^2\delta^3}(\chi^1, \chi^2, \chi^3) \;&\equiv\; e^{\boldsymbol{\iota}\frac{\pi}{2}(\mathbf{I}_\mathsf{y}^1+\mathbf{I}_\mathsf{y}^2+\mathbf{I}_\mathsf{y}^3)}\mathbf{R}_{\delta^1\delta^2\delta^3}(\chi^1, \chi^2, \chi^3)e^{-\boldsymbol{\iota}\frac{\pi}{2}(\mathbf{I}_\mathsf{y}^1+\mathbf{I}_\mathsf{y}^2+\mathbf{I}_\mathsf{y}^3)} \\ &=\; e^{-2\boldsymbol{\iota}(\delta^1\chi^1\mathbf{I}_\mathsf{z}^1+\delta^2\chi^2\mathbf{I}_\mathsf{z}^2+\delta^3\chi^3\mathbf{I}_\mathsf{z}^3)}\end{aligned} \tag{20}$$

This is because the idempotents $\mathbf{E}_\pm$ "absorb" the $\mathbf{I}_\mathsf{z}$ operators in the exponent, so that it can be expanded into a sum of terms involving only *scalar* exponentials,

$$\mathbf{R}'_{\delta^1\delta^2\delta^3}(\chi^1, \chi^2, \chi^3) \;=\; \mathbf{R}'_{\delta^1\delta^2\delta^3}(\chi^1, \chi^2, \chi^3)(\mathbf{E}_+^1 + \mathbf{E}_-^1)(\mathbf{E}_+^2 + \mathbf{E}_-^2)(\mathbf{E}_+^3 + \mathbf{E}_-^3) \tag{21}$$

where each term has the form

$$\mathbf{R}'_{\delta^1\delta^2\delta^3}(\chi^1, \chi^2, \chi^3)\mathbf{E}_{\epsilon^1}^1\mathbf{E}_{\epsilon^2}^2\mathbf{E}_{\epsilon^3}^3 \;\equiv\; e^{-\boldsymbol{\iota}(\epsilon^1\chi^1+\epsilon^2\chi^2+\epsilon^3\chi^3)}\mathbf{E}_{\epsilon^1}^1\mathbf{E}_{\epsilon^2}^2\mathbf{E}_{\epsilon^3}^3 \tag{22}$$

with $\epsilon^k \in \{-1, 0, +1\}$, $\epsilon^k = \delta^k\epsilon^k$ and $\mathbf{E}_0^k \equiv 1$ for $k = 1, 2, 3$. The average of each such scalar exponential is

$$\overline{e^{-\boldsymbol{\iota}(\epsilon^1\chi^1+\epsilon^2\chi^2+\epsilon^3\chi^3)}} \;=\; \int_{-\infty}^{\infty} P(\boldsymbol{\chi})e^{-\boldsymbol{\iota}\boldsymbol{\chi}\cdot\boldsymbol{\epsilon}}\mathrm{d}\boldsymbol{\chi} \;=\; e^{-\frac{t}{2}\boldsymbol{\epsilon}^\top\mathbf{C}\boldsymbol{\epsilon}}\;, \tag{23}$$

where $\boldsymbol{\epsilon} \equiv [\epsilon^1, \epsilon^2, \epsilon^3]^\top$. Since this is independent of the overall sign of $\boldsymbol{\epsilon}$, for $\boldsymbol{\epsilon} \neq \mathbf{0}$ the ensemble average of each $\mathbf{R}'_{\delta^1\delta^2\delta^3}(\chi^1, \chi^2, \chi^3)$ is a sum of pairs of terms of the form

$$e^{-\frac{t}{2}\boldsymbol{\epsilon}^\top\mathbf{C}\boldsymbol{\epsilon}}\left(\mathbf{E}_{\epsilon^1}^1\mathbf{E}_{\epsilon^2}^2\mathbf{E}_{\epsilon^3}^3 + \mathbf{E}_{-\epsilon^1}^1\mathbf{E}_{-\epsilon^2}^2\mathbf{E}_{-\epsilon^3}^3\right)\;. \tag{24}$$

In the case that $\epsilon^1 = \epsilon^2 = \epsilon^3 = 0$, Eq. (23) yields 1 as expected, while in the case that $\epsilon^j = \pm 1$ while the other two $\epsilon^i = 0$ $(1 \leq i \neq j \leq 3)$, the two terms in Eq. (24) are

$$\overline{e^{-2\boldsymbol{\iota}\chi^j\mathbf{I}_\mathsf{z}^j}} \;=\; e^{-\frac{t}{2}c^{jj}}(\mathbf{E}_+^j + \mathbf{E}_-^j) \;=\; e^{-tc^{jj}/2}\;. \tag{25}$$

In the case that $\epsilon^i = 0$ while ϵ^j and ϵ^k are nonzero ($\{i,j,k\} = \{1,2,3\}$), Eq. (24) has the form

$$e^{-\frac{t}{2}(c^{jj}+c^{kk}+2\epsilon^j\epsilon^k c^{jk})}(\mathbf{E}_{\epsilon^j}\mathbf{E}_{\epsilon^k} + \mathbf{E}_{-\epsilon^j}\mathbf{E}_{-\epsilon^k}) \tag{26}$$

where

$$(\mathbf{E}_{\epsilon^j}\mathbf{E}_{\epsilon^k} + \mathbf{E}_{-\epsilon^j}\mathbf{E}_{-\epsilon^k}) \;=\; \tfrac{1}{2}(1 + 4\epsilon^j\epsilon^k\mathbf{I}_{\mathsf{z}}^j\mathbf{I}_{\mathsf{z}}^k) \;\equiv\; \mathbf{E}_{\epsilon^j\epsilon^k}^{jk} \tag{27}$$

and $\mathbf{E}_{\pm}^{jk} \equiv \frac{1}{2}(1 \pm 4\mathbf{I}_{\mathsf{z}}^j\mathbf{I}_{\mathsf{z}}^k)$ is idempotent. Since there are two such pairs of terms, one with $\epsilon^j = \epsilon^k$ and the other with $\epsilon^j = -\epsilon^k$, the complete result is

$$\begin{aligned}
\overline{e^{-2\boldsymbol{\iota}(\chi^j\mathbf{I}_{\mathsf{z}}^j+\chi^k\mathbf{I}_{\mathsf{z}}^k)}} &= e^{-\frac{t}{2}(c^{jj}+c^{kk})}\left(e^{-t\,c^{jk}}\mathbf{E}_{+}^{jk} + e^{t\,c^{jk}}\mathbf{E}_{-}^{jk}\right) \\
&= e^{-\frac{t}{2}(c^{jj}+c^{kk})}\left(\cosh(t\,c^{jk}) - \sinh(t\,c^{jk})\,4\mathbf{I}_{\mathsf{z}}^j\mathbf{I}_{\mathsf{z}}^k\right) \\
&= e^{-\frac{t}{2}(c^{jj}+c^{kk}+8c^{jk}\mathbf{I}_{\mathsf{z}}^j\mathbf{I}_{\mathsf{z}}^k)}\,.
\end{aligned} \tag{28}$$

In a similar fashion, it can be shown that the average propagator for random rotations acting on the $8\mathbf{I}_{\mathsf{z}}^1\mathbf{I}_{\mathsf{z}}^2\mathbf{I}_{\mathsf{z}}^3$ term is

$$\overline{e^{-2\boldsymbol{\iota}(\chi^1\mathbf{I}_{\mathsf{z}}^1+\chi^2\mathbf{I}_{\mathsf{z}}^2+\chi^3\mathbf{I}_{\mathsf{z}}^3)}} \;=\; e^{-\frac{t}{2}(c^{11}+c^{22}+c^{33}+8c^{12}\mathbf{I}_{\mathsf{z}}^1\mathbf{I}_{\mathsf{z}}^2+8c^{13}\mathbf{I}_{\mathsf{z}}^1\mathbf{I}_{\mathsf{z}}^3+8c^{23}\mathbf{I}_{\mathsf{z}}^2\mathbf{I}_{\mathsf{z}}^3)} \tag{29}$$

These averages are easily rotated back to the average of the original propagator $\mathbf{R}_{\delta^1\delta^2\delta^3}(\chi^1,\chi^2,\chi^3)$ simply by replacing $\mathbf{I}_{\mathsf{z}}$ by $\mathbf{I}_{\mathsf{x}}$ throughout. All the terms obtained by the above expansions are collected in the next section.

5 Decoding and Error Correction

In order to write the ensemble average of Eq. (16) in a compact form, define the time-dependent (nonunitary) operators

$$F^j \;=\; F^j(t) \;\equiv\; e^{-t\,c^{jj}/2} \tag{30}$$

(acting by scalar multiplication), and

$$\mathbf{F}_{\mathsf{C}}^{jk} \;=\; \mathbf{F}_{\mathsf{C}}^{jk}(t) \;\equiv\; e^{-t\,c^{jk}4\mathbf{I}_{\mathsf{x}}^j\mathbf{I}_{\mathsf{x}}^k} \tag{31}$$

(acting by left-multiplication). Then the density matrix after decoherence becomes

$$\boldsymbol{\rho}_{\mathsf{C}} \;\equiv\; (\alpha + \beta 8\mathbf{I}_{\mathsf{x}}^1\mathbf{I}_{\mathsf{x}}^2\mathbf{I}_{\mathsf{x}}^3)\,\mathcal{F}_{\mathsf{C}}\left[\tfrac{1}{8}(1+F^1 2\mathbf{I}_{\mathsf{z}}^1)(1+F^2 2\mathbf{I}_{\mathsf{z}}^2)(1+F^3 2\mathbf{I}_{\mathsf{z}}^3)\right](\tilde{\alpha} + \tilde{\beta} 8\mathbf{I}_{\mathsf{x}}^1\mathbf{I}_{\mathsf{x}}^2\mathbf{I}_{\mathsf{x}}^3)\;, \tag{32}$$

where $\mathcal{F}_{\mathsf{C}}$ is a linear operator-valued function defined on the products of $\mathbf{I}_{\mathsf{z}}^k$ operators by

$$\begin{aligned}
\mathcal{F}_{\mathsf{C}}[\,1\,] &\equiv 1\;,\\
\mathcal{F}_{\mathsf{C}}[2\mathbf{I}_{\mathsf{z}}^j] &\equiv 2\mathbf{I}_{\mathsf{z}}^j \quad (1\le j\le 3)\;,\\
\mathcal{F}_{\mathsf{C}}[4\mathbf{I}_{\mathsf{z}}^j\mathbf{I}_{\mathsf{z}}^k] &\equiv \mathbf{F}_{\mathsf{C}}^{jk}\,4\mathbf{I}_{\mathsf{z}}^j\mathbf{I}_{\mathsf{z}}^k \quad (1\le j<k\le 3)\\
&\equiv e^{-t\,c^{jk}4\mathbf{I}_{\mathsf{x}}^j\mathbf{I}_{\mathsf{x}}^k}\,4\mathbf{I}_{\mathsf{z}}^j\mathbf{I}_{\mathsf{z}}^k\;,\\
\mathcal{F}_{\mathsf{C}}[8\mathbf{I}_{\mathsf{z}}^1\mathbf{I}_{\mathsf{z}}^2\mathbf{I}_{\mathsf{z}}^3] &\equiv \mathbf{F}_{\mathsf{C}}^{12}\mathbf{F}_{\mathsf{C}}^{13}\mathbf{F}_{\mathsf{C}}^{23}\,8\mathbf{I}_{\mathsf{z}}^1\mathbf{I}_{\mathsf{z}}^2\mathbf{I}_{\mathsf{z}}^3\\
&\equiv e^{-t\,c^{12}4\mathbf{I}_{\mathsf{x}}^1\mathbf{I}_{\mathsf{x}}^2 - t\,c^{13}4\mathbf{I}_{\mathsf{x}}^1\mathbf{I}_{\mathsf{x}}^3 - t\,c^{23}4\mathbf{I}_{\mathsf{x}}^2\mathbf{I}_{\mathsf{x}}^3}\,8\mathbf{I}_{\mathsf{z}}^1\mathbf{I}_{\mathsf{z}}^2\mathbf{I}_{\mathsf{z}}^3\;.
\end{aligned} \tag{33}$$

Next, the decoding operation is performed by applying the same two c-NOT's used in encoding, i.e. $\mathbf{S}^{23|1}$. On inserting appropriate factors of unity, the resulting density matrix can be written as

$$\begin{aligned}
\boldsymbol{\rho}_{\mathsf{D}} &\equiv (\alpha + \beta 2\mathbf{I}_{\mathsf{x}}^1)\mathcal{F}_{\mathsf{D}}\left[\tfrac{1}{8}\,\mathbf{S}^{23|1}(1+F^1 2\mathbf{I}_{\mathsf{z}}^1)(1+F^2 2\mathbf{I}_{\mathsf{z}}^2)(1+F^3 2\mathbf{I}_{\mathsf{z}}^3)\,\mathbf{S}^{23|1}\right](\tilde{\alpha} + \tilde{\beta} 2\mathbf{I}_{\mathsf{x}}^1) \qquad (34)\\
&= (\alpha + \beta 2\mathbf{I}_{\mathsf{x}}^1)\mathcal{F}_{\mathsf{D}}\left[\tfrac{1}{8}\,(1+F^1 2\mathbf{I}_{\mathsf{z}}^1)(1+F^2 4\mathbf{I}_{\mathsf{z}}^1\mathbf{I}_{\mathsf{z}}^2)(1+F^3 4\mathbf{I}_{\mathsf{z}}^1\mathbf{I}_{\mathsf{z}}^3)\right](\tilde{\alpha} + \tilde{\beta} 2\mathbf{I}_{\mathsf{x}}^1)\;,
\end{aligned}$$

where the linear operator-valued function $\mathcal{F}_{\mathsf{D}}$ is is defined on the products of $\mathbf{I}_{\mathsf{z}}^k$ operators by

$$\mathcal{F}_{\mathsf{D}}[\,\mathbf{S}^{23|1}\,\mathbf{X}\,\mathbf{S}^{23|1}\,] \;=\; \mathbf{S}^{23|1}\,\mathcal{F}_{\mathsf{C}}[\,\mathbf{X}\,]\,\mathbf{S}^{23|1}\;. \tag{35}$$

This translates to

$$\begin{aligned}
\mathcal{F}_{\mathsf{D}}[\,1\,] &\equiv 1\;,\\
\mathcal{F}_{\mathsf{D}}[2\mathbf{I}_{\mathsf{z}}^1] &\equiv 2\mathbf{I}_{\mathsf{z}}^1\;,\\
\mathcal{F}_{\mathsf{D}}[2\mathbf{I}_{\mathsf{z}}^2] &\equiv \mathbf{F}_{\mathsf{D}}^{12}\,2\mathbf{I}_{\mathsf{z}}^2 \;\equiv\; e^{-tc^{12}4\mathbf{I}_{\mathsf{x}}^1\mathbf{I}_{\mathsf{x}}^3}\,2\mathbf{I}_{\mathsf{z}}^2\;,\\
\mathcal{F}_{\mathsf{D}}[2\mathbf{I}_{\mathsf{z}}^3] &\equiv \mathbf{F}_{\mathsf{D}}^{13}\,2\mathbf{I}_{\mathsf{z}}^3 \;\equiv\; e^{-tc^{13}4\mathbf{I}_{\mathsf{x}}^1\mathbf{I}_{\mathsf{x}}^2}\,2\mathbf{I}_{\mathsf{z}}^3\;,
\end{aligned}$$

$$
\begin{aligned}
\mathcal{F}_{\mathsf{D}}[4\mathbf{I}_{\mathsf{z}}^1\mathbf{I}_{\mathsf{z}}^2] &\equiv 4\mathbf{I}_{\mathsf{z}}^1\mathbf{I}_{\mathsf{z}}^2\,, \qquad (36)\\
\mathcal{F}_{\mathsf{D}}[4\mathbf{I}_{\mathsf{z}}^1\mathbf{I}_{\mathsf{z}}^3] &\equiv 4\mathbf{I}_{\mathsf{z}}^1\mathbf{I}_{\mathsf{z}}^3\,,\\
\mathcal{F}_{\mathsf{D}}[4\mathbf{I}_{\mathsf{z}}^2\mathbf{I}_{\mathsf{z}}^3] &\equiv \mathbf{F}_{\mathsf{D}}^{23}\,4\mathbf{I}_{\mathsf{z}}^2\mathbf{I}_{\mathsf{z}}^3 \;\equiv\; e^{-tc^{23}4\mathbf{I}_{\mathsf{x}}^2\mathbf{I}_{\mathsf{x}}^3}\,4\mathbf{I}_{\mathsf{z}}^2\mathbf{I}_{\mathsf{z}}^3\,,\\
\mathcal{F}_{\mathsf{D}}[8\mathbf{I}_{\mathsf{z}}^1\mathbf{I}_{\mathsf{z}}^2\mathbf{I}_{\mathsf{z}}^3] &\equiv \mathbf{F}_{\mathsf{D}}^{12}\mathbf{F}_{\mathsf{D}}^{13}\mathbf{F}_{\mathsf{D}}^{23}\,8\mathbf{I}_{\mathsf{z}}^1\mathbf{I}_{\mathsf{z}}^2\mathbf{I}_{\mathsf{z}}^3\\
&\equiv e^{-tc^{12}4\mathbf{I}_{\mathsf{x}}^1\mathbf{I}_{\mathsf{x}}^3-tc^{13}4\mathbf{I}_{\mathsf{x}}^1\mathbf{I}_{\mathsf{x}}^2-tc^{23}4\mathbf{I}_{\mathsf{x}}^2\mathbf{I}_{\mathsf{x}}^3}\,8\mathbf{I}_{\mathsf{z}}^1\mathbf{I}_{\mathsf{z}}^2\mathbf{I}_{\mathsf{z}}^3\,,
\end{aligned}
$$

since

$$
\begin{aligned}
\mathbf{F}_{\mathsf{D}}^{jk} &\equiv \mathbf{S}^{23|1}e^{-t\,c^{jk}4\mathbf{I}_{\mathsf{x}}^j\mathbf{I}_{\mathsf{x}}^k}\mathbf{S}^{23|1} \;=\; e^{-t\,c^{jk}\mathbf{S}^{23|1}4\mathbf{I}_{\mathsf{x}}^j\mathbf{I}_{\mathsf{x}}^k\mathbf{S}^{23|1}} \qquad (37)\\
&= e^{-t\,c^{jk}4\mathbf{I}_{\mathsf{x}}^\ell\mathbf{I}_{\mathsf{x}}^m} \;=\; \begin{cases} e^{-t\,c^{12}4\mathbf{I}_{\mathsf{x}}^1\mathbf{I}_{\mathsf{x}}^3} & (j=1,k=2);\\ e^{-t\,c^{13}4\mathbf{I}_{\mathsf{x}}^1\mathbf{I}_{\mathsf{x}}^2} & (j=1,k=3);\\ e^{-t\,c^{23}4\mathbf{I}_{\mathsf{x}}^2\mathbf{I}_{\mathsf{x}}^3} & (j=2,k=3). \end{cases}
\end{aligned}
$$

Finally, the error correcting Toffoli gate $\mathbf{T}^{1|23} \equiv 2\mathbf{I}_{\mathsf{x}}^1\mathbf{E}_-^2\mathbf{E}_-^3 + (1 - \mathbf{E}_-^2\mathbf{E}_-^3)$ is applied. Since $\mathbf{T}^{1|23}$ commutes with the outer factors $\alpha + \beta\,2\mathbf{I}_{\mathsf{x}}^1$ and its conjugate, one could define a new function and work out how it operates on the transformed states as was done with $\mathcal{F}_{\mathsf{D}}$ above. Rather than simply permuting product operators as $\mathbf{S}^{23|1}$ does, however, $\mathbf{T}^{1|23}$ maps each to a linear combination of four products, and in order to evaluate the partial trace over the ancillae it is necessary to fully expand the result. Fortunately, this laborious task can be avoided by noting that for *any* product operator expression $\mathbf{X}$, the partial trace over the ancillae $4\langle\mathbf{X}\rangle^{23}$ is the same as $4\langle\mathcal{E}[\mathbf{X}]\rangle^{23}$

$$
\equiv\; 4\left\langle \mathbf{E}_+^2\mathbf{E}_+^3\,\mathbf{X}\,\mathbf{E}_+^2\mathbf{E}_+^3 + \mathbf{E}_+^2\mathbf{E}_-^3\,\mathbf{X}\,\mathbf{E}_+^2\mathbf{E}_-^3 + \mathbf{E}_-^2\mathbf{E}_+^3\,\mathbf{X}\,\mathbf{E}_-^2\mathbf{E}_+^3 + \mathbf{E}_-^2\mathbf{E}_-^3\,\mathbf{X}\,\mathbf{E}_-^2\mathbf{E}_-^3 \right\rangle^{23} \qquad (38)
$$

(This follows, for example, from the product operator characterization of the partial trace given in Ref. [**?**], Eq. (40).) In addition, the Toffoli commutes with all of the idempotents $\mathbf{E}_\pm^j$ $(j = 2, 3)$, so that $\mathcal{E}$ can be applied *before* applying the Toffoli gate. As shall be seen momentarily, this dramatically simplies the intermediate results, so that the linear combinations created on applying the final Toffoli are easily dealt with.

Because the idempotents $\mathbf{E}^j_\pm$ commute with $\mathbf{I}^k_\mathsf{z}$ for all $1 \le k \le j \le 3$, we can apply $\mathcal{E}$ directly to the coefficients $\mathbf{F}^{jk}_\mathsf{D}$ in Eq. (36), e.g.

$$\begin{aligned}
\mathcal{E}[\mathbf{F}^{12}_\mathsf{D}] &= \sum_{\epsilon^2,\,\epsilon^3\in\{\pm1\}} \mathbf{E}^2_{\epsilon^2}\mathbf{E}^3_{\epsilon^3}\left(\cosh(tc^{12}) - 4\mathbf{I}^1_\mathsf{x}\mathbf{I}^3_\mathsf{x}\sinh(tc^{12})\right)\mathbf{E}^2_{\epsilon^2}\mathbf{E}^3_{\epsilon^3} \qquad (39)\\
&= \sum_{\epsilon^2,\,\epsilon^3\in\{\pm1\}} \left(\cosh(tc^{12})\left(\mathbf{E}^2_{\epsilon^2}\mathbf{E}^3_{\epsilon^3}\right)^2 - 4\mathbf{I}^1_\mathsf{x}\mathbf{I}^3_\mathsf{x}\sinh(tc^{12})\left(\mathbf{E}^2_{\epsilon^2}\mathbf{E}^3_{-\epsilon^3}\right)\left(\mathbf{E}^2_{\epsilon^2}\mathbf{E}^3_{\epsilon^3}\right)\right)\\
&= \cosh(tc^{12})\sum_{\epsilon^2,\,\epsilon^3\in\{\pm1\}} \mathbf{E}^2_{\epsilon^2}\mathbf{E}^3_{\epsilon^3} \;=\; \cosh(tc^{12}) \;\equiv\; F^{12}\ .
\end{aligned}$$

In a similar fashion, it can be shown that

$$F^{13} \;\equiv\; \mathcal{E}[\mathbf{F}^{13}_\mathsf{D}] \;=\; \cosh(tc^{13})\ , \qquad\qquad F^{23} \;\equiv\; \mathcal{E}[\mathbf{F}^{23}_\mathsf{D}] \;=\; \cosh(tc^{23})\ , \qquad (40)$$

and $F^{123} \equiv$

$$\mathcal{E}[\mathbf{F}^{12}_\mathsf{D}\mathbf{F}^{13}_\mathsf{D}\mathbf{F}^{23}_\mathsf{D}] \;=\; \cosh(tc^{12})\cosh(tc^{13})\cosh(tc^{23}) - \sinh(tc^{12})\sinh(tc^{13})\sinh(tc^{23})\ . \qquad (41)$$

Thus applying the Toffoli to the projection of each term in Eq. (36) yields

$$\begin{aligned}
\mathbf{T}^{1|23}\mathcal{E}[\mathcal{F}_\mathsf{D}[\,1\,]]\mathbf{T}^{1|23} &= 1\ ,\\
\mathbf{T}^{1|23}\mathcal{E}[\mathcal{F}_\mathsf{D}[2\mathbf{I}^1_\mathsf{z}]]\mathbf{T}^{1|23} &= \mathbf{I}^1_\mathsf{z} + 2\mathbf{I}^1_\mathsf{z}\mathbf{I}^2_\mathsf{z} + 2\mathbf{I}^1_\mathsf{z}\mathbf{I}^3_\mathsf{z} - 4\mathbf{I}^1_\mathsf{z}\mathbf{I}^2_\mathsf{z}\mathbf{I}^3_\mathsf{z}\ ,\\
\mathbf{T}^{1|23}\mathcal{E}[\mathcal{F}_\mathsf{D}[2\mathbf{I}^2_\mathsf{z}]]\mathbf{T}^{1|23} &= F^{12}\,2\mathbf{I}^2_\mathsf{z}\ ,\\
\mathbf{T}^{1|23}\mathcal{E}[\mathcal{F}_\mathsf{D}[2\mathbf{I}^3_\mathsf{z}]]\mathbf{T}^{1|23} &= F^{13}\,2\mathbf{I}^3_\mathsf{z}\ , \qquad (42)\\
\mathbf{T}^{1|23}\mathcal{E}[\mathcal{F}_\mathsf{D}[4\mathbf{I}^1_\mathsf{z}\mathbf{I}^2_\mathsf{z}]]\mathbf{T}^{1|23} &= \mathbf{I}^1_\mathsf{z} + 2\mathbf{I}^1_\mathsf{z}\mathbf{I}^2_\mathsf{z} - 2\mathbf{I}^1_\mathsf{z}\mathbf{I}^3_\mathsf{z} + 4\mathbf{I}^1_\mathsf{z}\mathbf{I}^2_\mathsf{z}\mathbf{I}^3_\mathsf{z}\ ,\\
\mathbf{T}^{1|23}\mathcal{E}[\mathcal{F}_\mathsf{D}[4\mathbf{I}^1_\mathsf{z}\mathbf{I}^3_\mathsf{z}]]\mathbf{T}^{1|23} &= \mathbf{I}^1_\mathsf{z} - 2\mathbf{I}^1_\mathsf{z}\mathbf{I}^2_\mathsf{z} + 2\mathbf{I}^1_\mathsf{z}\mathbf{I}^3_\mathsf{z} + 4\mathbf{I}^1_\mathsf{z}\mathbf{I}^2_\mathsf{z}\mathbf{I}^3_\mathsf{z}\ ,\\
\mathbf{T}^{1|23}\mathcal{E}[\mathcal{F}_\mathsf{D}[4\mathbf{I}^2_\mathsf{z}\mathbf{I}^3_\mathsf{z}]]\mathbf{T}^{1|23} &= F^{23}\,4\mathbf{I}^2_\mathsf{z}\mathbf{I}^3_\mathsf{z}\ ,\\
\mathbf{T}^{1|23}\mathcal{E}[\mathcal{F}_\mathsf{D}[8\mathbf{I}^1_\mathsf{z}\mathbf{I}^2_\mathsf{z}\mathbf{I}^3_\mathsf{z}]]\mathbf{T}^{1|23} &= F^{123}\left(-\mathbf{I}^1_\mathsf{z} + 2\mathbf{I}^1_\mathsf{z}\mathbf{I}^2_\mathsf{z} + 2\mathbf{I}^1_\mathsf{z}\mathbf{I}^3_\mathsf{z} + 4\mathbf{I}^1_\mathsf{z}\mathbf{I}^2_\mathsf{z}\mathbf{I}^3_\mathsf{z}\right)
\end{aligned}$$

The partial trace over the ancilla simply drops all terms from the above that contain factors of $\mathbf{I}^2_\mathsf{z}$ or $\mathbf{I}^3_\mathsf{z}$, which eliminates all lines from the above equation containing a doubly-indexed

time-dependent coefficient F^{jk}. Multiplying each of the surviving terms by the appropriate scalar exponential $F^j \equiv \exp(-tc^{jj}/2)$ and combining finally yields

$$\begin{aligned}
\boldsymbol{\rho}_{\mathsf{E}}^1 &\equiv \langle \boldsymbol{\rho}_{\mathsf{E}} \rangle^{23} \equiv \Big\langle (\alpha + \beta\, 2\mathbf{I}_{\mathsf{x}}^1)\mathbf{T}^{1|23}\boldsymbol{\rho}_{\mathsf{D}}\mathbf{T}^{1|23}(\tilde{\alpha} + \tilde{\beta}\, 2\mathbf{I}_{\mathsf{x}}^1)\Big\rangle^{23} \\
&\equiv (\alpha + \beta\, 2\mathbf{I}_{\mathsf{x}}^1)\Big\langle \tfrac{1}{8}\,\mathbf{T}^{1|23}\mathcal{E}[\,\mathcal{F}_{\mathsf{D}}[\,1 + F^1\, 2\mathbf{I}_{\mathsf{z}}^1 + F^2\, 4\mathbf{I}_{\mathsf{z}}^1\mathbf{I}_{\mathsf{z}}^2 + F^3\, 4\mathbf{I}_{\mathsf{z}}^1\mathbf{I}_{\mathsf{z}}^3 \\
&\qquad + F^1F^2F^3\, F^{123}\, 8\mathbf{I}_{\mathsf{z}}^1\mathbf{I}_{\mathsf{z}}^2\mathbf{I}_{\mathsf{z}}^3\,]\,]\mathbf{T}^{1|23}\Big\rangle^{23}(\tilde{\alpha} + \tilde{\beta}\, 2\mathbf{I}_{\mathsf{x}}^1) \\
&= (\alpha + \beta\, 2\mathbf{I}_{\mathsf{x}}^1)\,\tfrac{1}{2}\left(1 + (F^1 + F^2 + F^3 - F^1F^2F^3\, F^{123})\mathbf{I}_{\mathsf{z}}^1\right)(\tilde{\alpha} + \tilde{\beta}\, 2\mathbf{I}_{\mathsf{x}}^1) \\
&= \tfrac{1}{2} + \Re(\tilde{\alpha}\beta)2\mathbf{I}_{\mathsf{x}}^1 + \left(\Im(\tilde{\alpha}\beta)2\mathbf{I}_{\mathsf{y}}^1 + (|\alpha|^2 - |\beta|^2)\mathbf{I}_{\mathsf{z}}^1\right)\Theta(t)\ ,
\end{aligned} \tag{43}$$

where

$$\begin{aligned}
\Theta(t) &\equiv \tfrac{1}{2}\,(\,F^1 + F^2 + F^3 - F^1F^2F^3\, F^{123}\,) \\
&\equiv \tfrac{1}{2}\,(\,e^{-tc^{11}/2} + e^{-tc^{22}/2} + e^{-tc^{33}/2}\,) - \tfrac{1}{8}\,e^{-tc^{11}/2}\,e^{-tc^{22}/2}\,e^{-tc^{33}/2}\ \times \\
&\qquad \left(e^{-tc^{12}-tc^{13}-tc^{23}} + e^{tc^{12}+tc^{13}-tc^{23}} + e^{tc^{12}-tc^{13}+tc^{23}} + e^{-tc^{12}+tc^{13}+tc^{23}}\right)\ .
\end{aligned} \tag{44}$$

This equation describes how the error-corrected state $\boldsymbol{\rho}_{\mathsf{E}}^1$ of the data spin #1 decays in the presence of decoherence due to external random fields about the x-axis, where $t\,c^{jj}$, $t\,c^{jk}$ are the variances and covariances among the phases of the three spins, as described in section **4** (Eq. (19)).

It is readily verified that the derivative $\dot{\Theta}(t)$ vanishes at $t = 0$ regardless of the covariances, as expected from the analysis given in section **2**. Two special cases are of particular interest in the following. The first occurs when the random phases χ^k are identically distributed and uncorrelated, so that $c^{11} = c^{22} = c^{33} \equiv 2/\tau$ and $c^{12} = c^{13} = c^{23} = 0$; then the above simplifies to:

$$\Theta(t) \;=\; \tfrac{1}{2}\,\left(\,3e^{-t/\tau} - e^{-3t/\tau}\,\right) \tag{45}$$

The second occurs when these random variables are totally correlated, so that $c^{jk} \equiv 2/\tau$ for $1 \le j \le k \le 3$; then:

$$\Theta(t) \;=\; \tfrac{1}{8}\,\left(\,9e^{-t/\tau} - e^{-9t/\tau}\,\right) \tag{46}$$

6 Discussion of Theoretical Results

Quantum error correcting codes were designed to prevent decoherence from occuring within a subsystem, at the expense of increasing decoherence in a quantum environment with which it interacts in a controllable fashion. In order to devise a quantum error correcting code, the mechanism of decoherence must be precisely known. Since a code can only correct for decay due to decoherence to first order (in the absence of concatenation [**?**]), decoherence can only be prevented over long time intervals if the error correction procedure can be performed much more rapidly than decoherence occurs. To do this, it is necessary to be able to rapidly reset the ancillae to their ground states after each correction so they can be reused, or else to have a large supply of ancillae in their ground states that can rapidly replace the used ones. Neither of these conditions is true in liquid-state NMR, since $T_1 \geq T_2$ and the number of spins whose interactions can be precisely controlled is limited.

Of course, pure states are not available at all in liquid-state NMR spectroscopy, as was assumed above for the ancillae. The isomorphism which exists between the dynamics of pure and pseudo-pure states ensures that error correction will nevertheless work, so long as the ancillae are in a pseudo-pure ground state relative to the data spin. As discussed in detail elsewhere [**?**, **?**], the preparation of the ancillae in a pseudo-pure state entails a loss of polarization that exceeds any potential gain through error correction, so that the net signal-to-noise in the NMR spectrum is actually lowered by the use of error correction. It would therefore be advantageous if a broader class of mixed states for the ancillae were also suitable for error correction, but arguments are given in an Appendix which imply that this is probably not true, and certainly not for any diagonal (z-polarized) mixed state of the ancillae.

In NMR, where decoherence occurs via a Raman process involving both translational and rotational molecular motions, measurements of the covariances in the fluctuating fields are important indicators of the nature of these motions. Thus, even though error correction cannot be used to sharpen the lines or improve signal-to-noise in NMR spectroscopy, the idea of coherently mixing together single and multiple quantum coherences so as to cancel the

first-order decay, under certain *specific* assumptions regarding the underlying mechanisms responsible for the relaxation and the correlations among them, clearly has the potential of being useful in NMR studies of molecular motions. The higher moments of the initial decay curve should also provide further confirmation of the assumptions. For example, the second derivative $\ddot{\Theta}(t)$ at $t = 0$ is $\ddot{\Theta}(0)$

$$= \; -\tfrac{1}{4}\left(2(c^{12})^2 + 2(c^{13})^2 + 2(c^{23})^2 + c^{11}c^{22} + c^{11}c^{33} + c^{22}c^{33}\right) \; < \; 0 \; , \tag{47}$$

while the third derivative is $\dddot{\Theta}(0)$

$$\begin{aligned} = \; & \tfrac{1}{16}\left(3(c^{11})^2(c^{22}+c^{33}) + 3(c^{22})^2(c^{11}+c^{33}) + 3(c^{33})^2(c^{22}+c^{33}) + 6(c^{11}c^{22}c^{33})\right. \\ & \left. + \; 12((c^{12})^2 + (c^{13})^2 + (c^{23})^2)(c^{11}+c^{22}+c^{33}) + 48(c^{12}c^{13}c^{23})\right) \; , \end{aligned} \tag{48}$$

which we expect will be generally positive.

Decoherence is of central importance to quantum mechanics, since it is the process by which classical statistical mechanics emerges from the underlying deterministic evolution of wave functions [**?**, **?**]. It is also a process which has proven extremely challenging to study in its full generality [**?**, **?**]. Although again somewhat limited by its ensemble nature, NMR is both theoretically and experimentally a very convenient model system in which to study decoherence. Because quantum codes only protect against decoherence by specific mechanisms, they can be used to design NMR experiments to test the validity of theoretical models. This will now be illustrated by describing liquid-state NMR experiments which validate the forgoing theoretical results.

7 Gradient Implementation of Decoherence

Loss of phase coherence is, of course, a natural relaxation process in NMR spectroscopy. The longitudinal fluctuating fields that induce this decoherence, however, come from many different sources, both intramolecular and intermolecular, and involving both spin and non-spin degrees of freedom. Superimposed on these longitudinal fluctuations are transverse fluctuations, which involve an exchange of energy with the environment. The three-bit

code majority logic analyzed above can deal with fluctuations about only one transverse axis; by including $\pi/2$ rotation and its inverse at the end of the encoding and beginning of the decoding, respectively, it can deal instead with longitudinal fluctuations. (Fluctuations about all three axes can only be corrected using at least four ancillae [**?**, **?**, **?**, **?**].) In addition, intramolecular dipole-dipole interactions are an important source of decoherence in liquid-state NMR, and these will also not be corrected by the three-bit code. Thus the forgoing theoretical results can only be rigorously demonstrated by experiments in which the dominant relaxation mechanism is a known, artificially induced fluctuation about a single transverse axis.

This is done here using molecular diffusion to randomize the spatial variations in the phase created by a pulsed field gradient. A field gradient along the z-axis causes the spins to precess at different rates, depending on their z-coordinates. This winds the transverse magnetization due to each coherence into a spiral, whose pitch decreases linearly with the length of the gradient pulse. In a liquid sample, the decay of a tightly wound spiral is due almost entirely to diffusion along its axis. Because the change in phase due to diffusion is exactly the same for every spin in a molecule, this implements the totally correlated error model.

The quantitative analysis of this process is best done using the k-space formalism [**?**]. The Fourier transform of the distribution of transverse magnetization $\upsilon(z)$ along the z-axis will be denoted here by $\Upsilon(k)$. The spiral produced by the gradient is described by the product $\upsilon(z)\exp(\imath n_{ij}k_0 z)$, where n_{ij} is the order of the coherence in question, whose Fourier transform is $\Upsilon(k)\delta(n_{ij}(k-k_0))$. Diffusion operates on the magnetization distribution by convolution with a Gaussian whose variance is $\sigma^2 = Dt$, where D is the diffusion coefficient [**?**], i.e. $\upsilon(z)\exp(\imath n_{ij}k_0 z) \star \exp(-z^2/(2\sigma))/\sqrt{2\pi\sigma^2}$. The Fourier transform is thus multiplied by the Gaussian $\exp(-(k-k_0)^2 n_{ij}^2 D/2)$, so that an inverse gradient pulse produces an echo which decays with the square of the coherence order, as expected from a totally correlated

dephasing process. These relations may be summarized as follows:

$$\begin{array}{ccccc} \upsilon(z) & \xrightarrow{\text{gradient}} & \upsilon(z)e^{-\imath n_{ij}k_0 z} & \xrightarrow{\text{diffusion}} & \upsilon(z)e^{-\imath n_{ij}k_0 z} \star e^{-z^2/2\sigma^2}/\sqrt{2\pi\sigma^2} \\ \updownarrow \text{FT} & & \updownarrow \text{FT} & & \updownarrow \text{FT} \\ \Upsilon(k) & \xrightarrow{\text{gradient}} & \Upsilon(k)\delta(n_{ij}(k-k_0)) & \xrightarrow{\text{diffusion}} & \Upsilon(k) \star \delta(n_{ij}(k-k_0))e^{-c_{ij}^2 k^2\sigma^2/2} \end{array} \tag{49}$$

Implementation of the uncorrelated error model was done by applying three successive gradient-diffusion sequences. In each sequence, two of the spins were refocussed during a gradient-pulse by selective RF π-pulses, while maintaining the phase ramp on the third spin (which was different in each of the three sequences). This was followed by a time interval to allow diffusion to randomize the phase of the third spin, after which a second gradient and further selective π-pulses were used to refocus all three spins (save for the coherence of the third lost to diffusion). This procedure randomized the phase of each spin equally and independently during separate diffusion intervals, as required by the uncorrelated model. The complex RF pulse and gradient sequences which performed this task are described in the following section.

8 Experimental Implementation of Error Correction

This section provides a detailed description of the RF and gradient pulse sequences used to implement the three-bit quantum error correcting code (see Fig. 1) as well as the correlated and uncorrelated decoherence models. The challenge here lies in obtaining precisely the desired effective Hamiltonian at each step, and in putting these steps together without side effects. In particular, the finite duration of all experimentally realizable RF and gradient pulses allow the system to evolve and so pick up wanted changes in the relative phases of its states. Therefore these unwanted evolutions must be refocussed, at the cost of increased complexity in the implementations. Additionally, the system is subjected to

incoherent errors due to pulse imperfections and field inhomogeneity. These could be compensated for by phase cycling and other averaging techniques [**?**, **?**], but this is undesirable in the present context since it complicates the interpretation of the experiments. Of course, such difficulties are not unique to NMR, but are expected to varying degrees in any quantum information processor. The intrinsically long decoherence times, innate averaging over ensembles and superb coherent control available in modern NMR spectroscopy is what makes these experiments possible today.

The three-bit quantum error correcting code was realized with a sample of ^{13}C-labeled alanine ($NH_3^+ - C^\alpha H(C^\beta H_3) - CO_2^-$) in D_2O solution at room temperature. The measurements were carried out on a Bruker AMX400 spectrometer (9.6 T) equipped with a 5 mm probe tuned to the ^{13}C and ^{1}H frequencies of 100.61 and 400.13 MHz, respectively. This probe was equipped with a z-gradient coils capable of generating field gradients of 60 G / cm. With decoupling of alanine's protons, this system exhibits a weakly-coupled carbon NMR spectrum. The internal Hamiltonian in the rotating frame is

$$\mathbf{H}_{\mathsf{int}} \;=\; \omega^{C'}\mathbf{I}_z^{C'} + \omega^{C^\alpha}\mathbf{I}_z^{C^\alpha} + \omega^{C^\beta}\mathbf{I}_z^{C^\beta} + 2\pi J^{C'C^\alpha}\mathbf{I}_z^{C'}\mathbf{I}_z^{C^\alpha} + 2\pi J^{C'C^\beta}\mathbf{I}_z^{C'}\mathbf{I}_z^{C^\beta} + 2\pi J^{C^\alpha C^\beta}\mathbf{I}_z^{C^\alpha}\mathbf{I}_z^{C^\beta} \quad (50)$$

where (with the transmitter on-resonance with the C^α)

$$\omega^{C'}/(2\pi) \;=\; 12580\text{Hz}, \;\; \omega^{C^\alpha}/(2\pi) \;=\; 0\text{Hz}, \;\; \omega^{C^\beta}/(2\pi) \;=\; -3443\text{Hz}, \quad (51)$$

$$J^{C'C^\alpha} \;=\; 54.2\text{Hz}, \quad J^{C'C^\beta} \;=\; 1.2\text{Hz}, \quad J^{C^\alpha C^\beta} \;=\; 35.1\text{Hz}\ .$$

The C^α was chosen as the data spin #1, and exhibits a well-resolved quartet in the spectrum. This has the advantage that none of the gates required for the error correction procedure needed to use the small 1.2 Hz coupling directly (although it was necessary to refocus this coupling). The carbonyl C' (spin #2) and C^β (spin #3) were used for the two ancilla spins.

To implement a universal set of quantum logic gates in a spin system it is sufficient that all the spins be connected by coupling pathways and sufficiently well-resolved to enable arbitary rotations to be applied to any subset of the spins. Here selective excitations were implemented using phase-modulated Gaussian pulses [**?**]. These shaped pulses consisted of 384 complex points with a total duration of 1.5 msec, with an excitation profile that

consisted of Gaussians centered on the frequencies of the (one or more) spins of interest with a standard deviation of 500 Hz. The transmitter was placed on the data spin, enabling it to be controlled by soft rectangular pulses.

It is convenient to define five specific pulse sequences, which were designed to yield a simple, well-defined effective Hamiltonian and served as the "modules" (building-blocks) for the overall pulse sequences. In the following list, all the time intervals are calculated from the midpoints of their surrounding shaped pulses.

Identity(t): This is a "time-suspension" sequence which is designed to refocus all components of the Hamiltonian by the symmetric application of π-pulses [**?**]. Identity sequences correct the phase errors due to the finite duration of RF and gradient pulses, and are used whenever two noncommuting operations must be applied sequentially. The implementation used in these experiments is given by the pulse sequence (in left-to-right temporal order)

$$\left(\pi\right)^{k\ell} - \left(\pi\right)^{\ell m} - \left(-\pi\right)^{k\ell} - \left(\Delta\right) - \left(\pi\right)^{k\ell} - \left(-\pi\right)^{\ell m} - \left(-\pi\right)^{k\ell}, \tag{52}$$

where $(\pi)^{k\ell}$ denotes a π-rotation of spins k, ℓ about the x-axis, and similarly for $(\pi)^{\ell m}$ and $(\pi)^{km}$. These pulses have a duration of Δ, so that the net propagator can be written as e.g.

$$\left(\pi\right)^{k\ell} \quad \Leftrightarrow \quad e^{-\boldsymbol{\iota}\mathbf{H}_{\mathsf{int}}\Delta/2} e^{-\boldsymbol{\iota}\pi(\mathbf{I}_{\mathsf{x}}^{k}+\mathbf{I}_{\mathsf{x}}^{\ell})} e^{-\boldsymbol{\iota}\mathbf{H}_{\mathsf{int}}\Delta/2} \tag{53}$$

with similar expressions for the other pulses. Thus if one places such an identity sequence between two noncommuting pulses, the evolution during the $\Delta/2$ duration of the last half of the first pulse and the first half of the last pulse (as in Eq. (53)) cancels with the evolution during the intervening identity sequence. Note that due to the symmetry of this sequence all the CH couplings are refocussed, so that additional decoupling of the protons is not needed.

Jdelay(k, ℓ, t): This module yields the effective Hamiltonian $2\pi J^{kl}\mathbf{I}_{\mathsf{z}}^{k}\mathbf{I}_{\mathsf{z}}^{\ell}$ where $k, l = 1, 2, 3$ are spin indices. The parameter t determines the net acquired phase $\varphi = 2\pi J^{k\ell} t$; if $k = 1$, $\ell = 2$, for example, a phase shift of φ is obtained from $t = \varphi/(2J^{12}) = \varphi/(2 \times 54.2)$ sec. The complete sequence is

$$\left(\frac{t}{4}\right) - \left(\pi\right)^{123} - \left(\frac{t}{4}\right) - \left(\pi\right)^{k\ell} - \left(\frac{t}{4}\right) - \left(-\pi\right)^{123} \tag{54}$$

$$-\left(\frac{t}{4}\right)-\left(\Delta\right)-\left(\pi\right)^{km}-\left(-\pi\right)^{k\ell}-\left(-\pi\right)^{km}\quad,$$

where $[\Delta]$ is again a delay of duration equal to that of the shaped pulses (1.5 msec.). The finite duration of the pulses sets a lower limit for the phase evolution of $\varphi > 4\cdot 2\cdot J^{k\ell}\Delta$ ($= 0.21\pi$ for J^{12} and 0.13π for J^{13}).

JdelayInv(k,ℓ,t): This is a short version of *Jdelay* with one modification: after its application all three spins are inverted by π relative to the result of *Jdelay*. Successive evolutions under $2\pi J^{12}\mathbf{I}_z^1\mathbf{I}_z^2$ and $2\pi J^{13}\mathbf{I}_z^1\mathbf{I}_z^3$ were often needed in these experiments, and the same result is obtained from using two successive *JdelayInv* modules as from two successive Jdelay modules. The former, however, saves three shaped pulses, as may be seen from its pulse sequence:

$$\left(\frac{t}{4}\right)-\left(\pi\right)^{k\ell}-\left(\frac{t}{4}\right)-\left(\pi\right)^{123}-\left(\frac{t}{4}\right)-\left(-\pi\right)^{k\ell}-\left(\frac{t}{4}\right) \tag{55}$$

TC-Decohere(g,δ,t,T): This module was used to induce decoherence under totally correlated external random fields. It includes two gradients of equal strength g and duration δ but opposite polarity, embedded in a time-suspension sequence of length T. The gradients are separated by a period t during which diffusion takes place. The effects of decoherence due to T_2 relaxation during this module were reduced to a constant factor by keeping the total time required fixed at T while varying t. Letting $[\mathsf{z}\text{−grad}(g,\delta)]$ denote a gradient pulse along the z-axis of strength g and duration δ, the pulse sequence used for this module was

$$\begin{aligned}&\left(\frac{T}{8}\right)-\left(\pi\right)^{km}-\left(\frac{T}{8}\right)-\left(\pi\right)^{k\ell}-\left(\frac{T}{8}\right)-\left(-\pi\right)^{km}-\left(\frac{T}{8}-\frac{t}{2}-\frac{\delta}{2}\right)\\ &-\left(\mathsf{z}\text{−grad}(g,\delta)\right)-\left(\frac{t}{2}-\frac{\delta}{2}\right)-\left(\Delta\right)-\left(\frac{t}{2}-\frac{\delta}{2}\right)-\left(\mathsf{z}\text{−grad}(-g,\delta)\right)\\ &-\left(\frac{T}{8}-\frac{t}{2}-\frac{\delta}{2}\right)-\left(\pi\right)^{km}-\left(\frac{T}{8}\right)-\left(-\pi\right)^{k\ell}-\left(\frac{T}{8}\right)-\left(-\pi\right)^{km}-\left(\frac{T}{8}\right)\end{aligned} \tag{56}$$

This pulse sequence is shown in diagrammatic form in Fig. 2(a).

UC-Decohere(g,δ,r_2,r_1): This module was used to induce decoherence under uncorrelated external random fields (see above). It uses a combination of refocusing and gradient pulses of absolute strength g and duration δ. These gradient pulses were strung together into one

of three sequences, all of the form

$$G^i: \quad \Big(\mathsf{z}{-}\mathrm{grad}(g_1^i,\delta)\Big) - \Big(\pi\Big)^{12} - \Big(\mathsf{z}{-}\mathrm{grad}(g_2^i,\delta)\Big) - \Big(\pi\Big)^{13} - \Big(\mathsf{z}{-}\mathrm{grad}(g_3^i,\delta)\Big) - \Big(\pi\Big)^{12} - \Big(\mathsf{z}{-}\mathrm{grad}(g_4^i,\delta)\Big) - \Big(\pi\Big)^{13}\ , \tag{57}$$

where the polarities in the sequence g^i for dephasing the i-th spin were given by

$$\begin{aligned} g^1: &\quad [+g,\,-g,\,+g,\,-g] \\ g^2: &\quad [+g,\,-g,\,-g,\,+g] \\ g^3: &\quad [+g,\,+g,\,-g,\,-g]\ . \end{aligned} \tag{58}$$

Each of these gradient sequences, in turn, was embedded in a fixed number of repetitions of a sequence of refocusing pulses, of the form

$$\Big(\delta\Big) - \Big(\pi\Big)^{12} - \Big(\delta\Big) - \Big(\pi\Big)^{13}\ , \tag{59}$$

where (δ) indicates a time delay. Note that two consecutive repetitions of this sequence refocuses both the chemical shift and coupling evolution, and that the sequences G^i above with $g = 0$ comprise two such repetitions and so do nothing, as desired. A given number R of repetitions of this pulse sequence will be denoted by (R), while the gradient sequence which refocuses the effects of the gradient sequence (G^i) in a given experiment will be denoted by $(\tilde{G}^i)$. Depending on whether the intervening number of refocusing sequences (59) is even or odd, this will either be (G^i) or the same sequence with all its polarities reversed. Thus the overall sequence used to independently decohere all three spins and thereby implement the uncorrelated decoherence model is given by

$$\Big(r_2 - r_1\Big) - \Big(G^1\Big) - \Big(r_1\Big) - \Big(\tilde{G}^1\Big) - \Big(r_2 - r_1\Big) - \Big(G^2\Big) - \Big(r_1\Big) - \Big(\tilde{G}^2\Big) - \Big(r_2 - r_1\Big) - \Big(G^3\Big) - \Big(r_1\Big) - \Big(\tilde{G}^3\Big)\ , \tag{60}$$

where $0 < r_1 < r_2$ are integers and (r_1) or $(r_2 - r_1)$ denote the enclosed number of repetitions of (59). This pulse sequence is shown in diagrammatic form in Fig. 2(b). Observe the total length of each experiment is constant, which keeps the effect of intrinsic T_2 relaxation to a

constant overall factor. The signal loss due to RF inhomogeneity during the application of the long train of refocusing pulses is reduced by a CPMG type phase modulation of length eight [**?**]. These phase changes are carried out during a single scan of each experiment, and no phase cycling is performed across scans.

In the TC-Decohere module, the gradient strength and duration were $g = 35.7$ Gauss/cm and $\delta = 2.5$ msec., respectively, while the total time was kept fixed at $T = 64.5$ msec. with a diffusion time increment of $t = 4$ msec. In the UC-Decohere module, the gradient strength used was $|g| = 12.2$ Gauss/cm, with $\delta = 2.078$ msec., which yields an increment of 7.156 msec. over $r_2 = 21$ time points.

An account of how to design pulse sequences, composed of these modules, for any desired effective Hamiltonian may be found in our earlier work [**?**, **?**]. For the sake of completeness, however, the basic ideas are repeated for the case of the error-correcting Toffoli gate. This gate may be written in exponential form and expanded into a product of commuting propagators, as follows:

$$\begin{aligned} \mathbf{T}^{1|23} &\equiv 2\mathbf{I}_{\mathsf{x}}^{1}\mathbf{E}_{-}^{2}\mathbf{E}_{-}^{3} + (1 - \mathbf{E}_{-}^{2}\mathbf{E}_{-}^{3}) \;=\; e^{\boldsymbol{\iota}\pi(1/2 - \mathbf{I}_{\mathsf{x}}^{1}\mathbf{E}_{-}^{2}\mathbf{E}_{-}^{3})\mathbf{E}_{-}^{2}\mathbf{E}_{-}^{3}} \\ &= e^{\boldsymbol{\iota}\pi/8}\, e^{-\boldsymbol{\iota}\pi/4\mathbf{I}_{\mathsf{x}}^{1}}\, e^{-\boldsymbol{\iota}\pi/4\mathbf{I}_{\mathsf{z}}^{2}}\, e^{-\boldsymbol{\iota}\pi/4\mathbf{I}_{\mathsf{z}}^{2}}\, e^{\boldsymbol{\iota}\pi/2\mathbf{I}_{\mathsf{x}}^{1}\mathbf{I}_{\mathsf{z}}^{2}}\, e^{\boldsymbol{\iota}\pi/2\mathbf{I}_{\mathsf{x}}^{1}\mathbf{I}_{\mathsf{z}}^{3}}\, e^{\boldsymbol{\iota}\pi/2\mathbf{I}_{\mathsf{z}}^{2}\mathbf{I}_{\mathsf{z}}^{3}}\, e^{-\boldsymbol{\iota}\pi\mathbf{I}_{\mathsf{x}}^{1}\mathbf{I}_{\mathsf{z}}^{2}\mathbf{I}_{\mathsf{z}}^{3}} \end{aligned} \tag{61}$$

The propagators in this expression could be further expanded into products of propagators directly implementable using the above modules. In these experiments, however, the Toffoli gate is followed immediately by a partial trace over the ancillae, i.e. by observing the data spin while decoupling the ancillae. Hence all propagators that operate only on the ancillae can be eliminated with no effect on the final result. Since the net phase is also unobservable, this leaves only the product of the propagators

$$e^{-\boldsymbol{\iota}\pi/4\mathbf{I}_{\mathsf{x}}^{1}}\, e^{\boldsymbol{\iota}\pi/2\mathbf{I}_{\mathsf{x}}^{1}\mathbf{I}_{\mathsf{z}}^{2}}\, e^{\boldsymbol{\iota}\pi/2\mathbf{I}_{\mathsf{x}}^{1}\mathbf{I}_{\mathsf{z}}^{3}}\, e^{-\boldsymbol{\iota}\pi\mathbf{I}_{\mathsf{x}}^{1}\mathbf{I}_{\mathsf{z}}^{2}\mathbf{I}_{\mathsf{z}}^{3}} \;. \tag{62}$$

This in turn can be implemented by the sequence of propagators of the effective Hamiltonians (in reverse temporal order):

$$e^{\boldsymbol{\iota}\pi/4\mathbf{I}_{\mathsf{x}}^{1}}\, e^{\boldsymbol{\iota}\pi/2\mathbf{I}_{\mathsf{z}}^{1}}\, e^{\boldsymbol{\iota}\pi\mathbf{I}_{\mathsf{z}}^{1}\mathbf{I}_{\mathsf{z}}^{2}}\, e^{-\boldsymbol{\iota}\pi\mathbf{I}_{\mathsf{y}}^{1}}\, e^{\boldsymbol{\iota}\pi/2\mathbf{I}_{\mathsf{z}}^{1}\mathbf{I}_{\mathsf{z}}^{3}}\, e^{-\boldsymbol{\iota}\pi/2\mathbf{I}_{\mathsf{y}}^{1}}\, e^{\boldsymbol{\iota}\pi\mathbf{I}_{\mathsf{z}}^{1}\mathbf{I}_{\mathsf{z}}^{2}}\, e^{\boldsymbol{\iota}\pi/2\mathbf{I}_{\mathsf{x}}^{1}}\, e^{\boldsymbol{\iota}7\pi/2\mathbf{I}_{\mathsf{z}}^{1}\mathbf{I}_{\mathsf{z}}^{2}}\, e^{-\boldsymbol{\iota}\pi\mathbf{I}_{\mathsf{y}}^{1}}\, e^{\boldsymbol{\iota}\pi/2\mathbf{I}_{\mathsf{z}}^{1}\mathbf{I}_{\mathsf{z}}^{3}}\, e^{-\boldsymbol{\iota}\pi/2\mathbf{I}_{\mathsf{y}}^{1}} \tag{63}$$

These effective Hamiltonians can all be obtained by combining the above modules with RF pulses.

The state $\mathbf{I}_{\mathsf{z}}^1\mathbf{E}_+^2\mathbf{E}_+^3$ was prepared first, after which the other states $\mathbf{I}_{\mathsf{x}}^1\mathbf{E}_+^2\mathbf{E}_+^3$ and $\mathbf{I}_{\mathsf{y}}^1\mathbf{E}_+^2\mathbf{E}_+^3$ used in the experiments were obtained by rotating spin #1. Starting with the three-spin equilibrium state $\mathbf{I}_{\mathsf{z}}^1 + \mathbf{I}_{\mathsf{z}}^2 + \mathbf{I}_{\mathsf{z}}^3$, a pair of c-NOT's was applied to the ancillae conditional on the data spin:

$$\mathbf{S}^{2|1}\mathbf{S}^{3|1}\left(\mathbf{I}_{\mathsf{z}}^1 + \mathbf{I}_{\mathsf{z}}^2 + \mathbf{I}_{\mathsf{z}}^3\right)\mathbf{S}^{3|1}\mathbf{S}^{2|1} \;=\; \mathbf{I}_{\mathsf{z}}^1(1 + 2\mathbf{I}_{\mathsf{z}}^2 + 2\mathbf{I}_{\mathsf{z}}^3) \tag{64}$$

This was then subjected to the pulse sequence (given in temporal order)

$$\left(\tfrac{\pi}{2}\right)^1 - \left(\tfrac{1}{4J^{12}}\right) - \left(\tfrac{\pi}{2}\right)^1_{\pi/4} - (\mathsf{x}{-}\mathrm{grad}) - \left(\tfrac{\pi}{2}\right)^1_{\pi/4} - \left(\tfrac{1}{4J^{13}}\right) - \left(\tfrac{\pi}{2}\right)^1_{\pi/2} - (\mathsf{y}{-}\mathrm{grad}) \;, \tag{65}$$

where $[1/(2J^{1k})]$ is an evolution under the effective Hamiltonian $2\pi J^{1k}\mathbf{I}_{\mathsf{z}}^1\mathbf{I}_{\mathsf{z}}^k$ a time $1/(2J^{1k})$ $(k = 2, 3)$, i.e. $Jdelay(1, k, t)$, $(\mathsf{x}{-}\mathrm{grad})$ is a magnetic field gradient of $\partial B_{\mathsf{z}}/\partial x$, and similarly for $(\mathsf{y}{-}\mathrm{grad})$. This yields $3\mathbf{I}_{\mathsf{z}}^1\mathbf{E}_+^2\mathbf{E}_+^3$. Note that this method of preparation reduces the signal of the data spin by 25% (as opposed to the 50% expected from the equilibrium populations [**?**]); the transformation in Eq. (65) also has the interesting property of being a projection, in that applying it a second time to the resulting state does not change the state.

The final operation required is to observe the partial trace over the ancillae at the end. Because only single quantum coherences of the form $\mathbf{I}_{\mathsf{x}}^k$ and $\mathbf{I}_{\mathsf{y}}^k$ are observable, to implement the partial trace during acquisition it is only necessary to prevent antiphase magnetization with respect to the ancillae from evolving into observable single quantum terms. This was achieved by interspersing the sampling of the signal with π-pulses on the ancillae, thereby repeatedly refocusing these terms. This RF irradiation caused a fixed upfield shift of ~ 12 Hz due to the Bloch-Seigert effect [**?**].

9 Experimental Results and Discussion

The error correcting code shown in Fig. 1 was applied to the $\mathbf{I}_{\mathsf{x}}^1\mathbf{E}_+^2\mathbf{E}_+^3$, $\mathbf{I}_{\mathsf{y}}^1\mathbf{E}_+^2\mathbf{E}_+^3$ and $\mathbf{I}_{\mathsf{z}}^1\mathbf{E}_+^2\mathbf{E}_+^3$ states. One can regard this code as a modification of the classical majority logic code for

protecting against bit flip errors about the x-axis. It follows that the $\mathbf{I}_x^1\mathbf{E}_+^2\mathbf{E}_+^3$ should not be affected by the gradient induced decoherence, whereas both $\mathbf{I}_y^1\mathbf{E}_+^2\mathbf{E}_+^3$ and $\mathbf{I}_z^1\mathbf{E}_+^2\mathbf{E}_+^3$ will decay exponentially at the same rate in the absence of error correction. These exponential decay rates were measured by applying the gradient diffusion procedure directly to the $\mathbf{I}_y^1$ and $\mathbf{I}_z^1$ states, respectively.

In Figs. 3 and 4, the decay of the magnetization of the data spin is plotted with and without the error correction procedure starting from the $\mathbf{I}_z^1\mathbf{E}_+^2\mathbf{E}_+^3$ and $\mathbf{I}_y^1\mathbf{E}_+^2\mathbf{E}_+^3$ states, respectively. In both these experiments the initial slope of the error corrected curve tends to zero as the decoherence time $t \to 0$, in accord with theoretical predictions. This was quantified by using the rate $1/\tau$ of the uncorrected decay, estimated from a linear least-squares fit to its logarithm, to predict the corrected decay curve from equation for totally correlated decoherence $(9\exp(-t/\tau) - \exp(-9t/\tau))/8$ (see Eq. (46)). The correlation coefficient between the measured and predicted amplitudes were 0.9845 and 0.9704 for the $\mathbf{I}_z^1\mathbf{E}_+^2\mathbf{E}_+^3$ and $\mathbf{I}_y^1\mathbf{E}_+^2\mathbf{E}_+^3$ experiments, respectively. In the figures, the error-corrected data points have been scaled so that their mean-square value is the same as that of the corresponding predicted points; no other free parameters were needed for these fits.

The scatter seen in the data points, typically about $\pm 1\%$ of the peak intensity after averaging of 16 repetitions, can be attributed primarily to RF field inhomogeneity, particularly during the long period of induced decoherence. In Fig. 5, we also show the amplitudes of the peak starting from the $\mathbf{I}_x^1\mathbf{E}_+^2\mathbf{E}_+^3$ data spin state, from which it is evident that it is not significantly affected by the overall error correction procedure. The apparent decay rate of ≈ 0.2 sec^{-1} can likewise be attributed primarily to RF field inhomogeneity, which produced a small transverse magnetization after encoding.

Figure 6 shows the results of a similar set of experiments on the $\mathbf{I}_z^1\mathbf{E}_+^2\mathbf{E}_+^3$ state, with independent diffusion intervals for each of the three spins to implement uncorrelated decoherence, as previously described. As in the correlated experiments, the decay rate $1/\tau$ obtained from a least-squares fit to the logarithm of the decay of the $\mathbf{I}_x^1\mathbf{E}_+^2\mathbf{E}_+^3$ state due to this decoherence procedure was used to calculate the theoretical curve $(3\exp(-t/\tau) - \exp(-3t/\tau))/2$ (see Eq. (45)), and scaled the corresponding error-corrected data to have the same root-mean-square

as the theoretical curve sampled at the corresponding time points. Although the experimental difficulties of juxtaposing three independent gradient-decoherence sequences without picking up unwanted phase shifts induces appreciable nonrandom scatter in the data points, the fit is once again in accord with theoretical predictions. Also shown with a dashed line is the decay curve expected for totally correlated decoherence, showing that these experiments are indeed capable of distinguishing these two cases.

Together, these results provide strong support not only for the theory of quantum error correction, but also for the ability of pseudo-pure states to reproduce the dynamics of true pure states. This ability is important because liquid-state NMR spectroscopy provides a degree of coherent control that is presently more difficult to obtain in other quantum systems of comparable complexity. Although limited to about ten spins [**?**, **?**] and hence within reach of classical computer simulations, such an experimentally accessible paradigm for quantum information processing should be quite useful particularly in the study of decoherence [**?**]. It forces one to consider, and enables one to experimentally determine, actual relaxation superoperators, rather than working from idealized theoretical models of decoherence. The development of error correcting codes that can handle such real-life decoherence is a significant challenge whose solution is likely to be applicable to quantum information processing in other systems.

Conversely, the theory of quantum error correction promises to lead to new methods for studying molecular dynamics through the relaxation of multiple quantum coherences [**?**, **?**, **?**, **?**, **?**, **?**]. This may be seen, for example, by considering the second derivative of the error-corrected curves at $t = 0$ in the uncorrelated and totally correlated cases, which are $-3/\tau^2$ and $-9/\tau^2$, respectively, while the corresponding inflection points occur at $\ln(3)\tau/2$ and $\ln(3)\tau/4$. Moreover, since the covariances of the random fields at the three spins occur in our formulae for the decay of the error-corrected states, it would appear possible to derive these covariances directly from sufficiently detailed measurements. One of the goals of on-going studies of quantum error correction by the present authors is to develop codes which can more clearly reveal the nature of the underlying spin and molecular dynamics, for example by correcting for dipole-dipole relaxation. Work in these directions is currently in progress.

Acknowledgements

This work was supported by the U. S. Army Research Office under grant number DAAG 55-97-1-0342 from the DARPA Microsystems Technology Office.

Appendix: Error Correction in Mixed States

This appendix shows that error correction will not be able to correct the first-order decay of the data spin in any diagonal mixed state for the ancillae save for their pseudo-pure ground state, unless the state of the data spin is taken into account. Assuming that the ancillae are initially uncorrelated with the data spin, such a state may be written as

$$\boldsymbol{\rho} \;=\; \boldsymbol{\rho}^1_{\mathsf{A}} \left(\mu_{++}\mathbf{E}^2_+\mathbf{E}^3_+ + \mu_{+-}\mathbf{E}^2_+\mathbf{E}^3_- + \mu_{-+}\mathbf{E}^2_-\mathbf{E}^3_+ + \mu_{--}\mathbf{E}^2_-\mathbf{E}^3_-\right) \tag{66}$$

with nonnegative coefficients satisfying $\mu_{++}+\mu_{+-}+\mu_{-+}+\mu_{--}=1$. For each term $\boldsymbol{\rho}^1_{\mathsf{A}}\mathbf{E}^2_{\epsilon^2}\mathbf{E}^3_{\epsilon^3}$ obtained upon expansion, the only change in the preceding results (Eq. (43)) is that the signs of the coefficients F^2 & F^3 are given by ϵ^2 & ϵ^3, so the partial trace after error correction is

$$\boldsymbol{\rho}^1_{\mathsf{E}} \;=\; \tfrac{1}{2} + \nu_{\mathsf{x}} 2\mathbf{I}^1_{\mathsf{x}} + \left(\nu_{\mathsf{y}} 2\mathbf{I}^1_{\mathsf{y}} + \nu_{\mathsf{z}} 2\mathbf{I}^1_{\mathsf{z}}\right)\Theta'(t)\ , \tag{67}$$

where the partial trace is initially

$$\boldsymbol{\rho}^1_{\mathsf{A}} \;=\; \tfrac{1}{2} + \nu_{\mathsf{x}} 2\mathbf{I}^1_{\mathsf{x}} + \nu_{\mathsf{y}} 2\mathbf{I}^1_{\mathsf{y}} + \nu_{\mathsf{z}} 2\mathbf{I}^1_{\mathsf{z}} \tag{68}$$

and now $\Theta'(t) =$

$$\begin{aligned} &\tfrac{1}{2}\big(F^1 + (\mu_{++}+\mu_{+-}-\mu_{-+}-\mu_{--})F^2 + (\mu_{++}-\mu_{+-}+\mu_{-+}-\mu_{--})F^3 \\ &\quad -(\mu_{++}-\mu_{+-}-\mu_{-+}+\mu_{--})F^1F^2F^3\,F^{123}\big)\ . \end{aligned} \tag{69}$$

The derivative at $t=0$ is $\dot{\Theta}'(0) =$

$$\tfrac{1}{4}\left((\mu_{++}-1)c^{11} - \mu_{+-}(c^{11}+2c^{22}) - \mu_{-+}(c^{11}+2c^{33}) + \mu_{--}(c^{11}+2c^{22}+2c^{33})\right)\ , \tag{70}$$

and for $c^{11}\neq 0$ the only nonnegative solution to this equation together with the normalization condition is $\mu_{++}=1$ and $\mu_{+-}=\mu_{-+}=\mu_{--}=0$. This proves that, in any such state, the

three-bit error correcting code (Fig. 1) will inhibit decoherence to first order only if the ancillae are in a psuedo-pure state relative to the data spin.

More generally, consider a mixed state in which the ancillae are diagonal but (classically) correlated with the data spin, i.e.

$$\begin{aligned} \boldsymbol{\rho} &= \sum\nolimits_m \mu_m \, \boldsymbol{\rho}^1_m \, \mathbf{E}^2_{\epsilon^2_m} \, \mathbf{E}^3_{\epsilon^3_m} \\ &= \boldsymbol{\rho}^1_{++} \mathbf{E}^2_+ \mathbf{E}^3_+ + \boldsymbol{\rho}^1_{+-} \mathbf{E}^2_+ \mathbf{E}^3_- + \boldsymbol{\rho}^1_{-+} \mathbf{E}^2_- \mathbf{E}^3_+ + \boldsymbol{\rho}^1_{--} \mathbf{E}^2_- \mathbf{E}^3_- \ , \end{aligned} \tag{71}$$

where $\boldsymbol{\rho}^1_{++} \equiv \sum_{\{m|\epsilon^2_m=\epsilon^3_m=1\}} \mu_m \boldsymbol{\rho}^1_m$, etc., and $\sum_m \mu_m = 1$ ($\mu_m \geq 0$). Letting $\upsilon_{\epsilon^2\epsilon^3} \equiv \left\langle \boldsymbol{\rho}^1_{\epsilon^2\epsilon^3} 2\mathbf{I}^1_{\mathsf{y}} \right\rangle$ and $\zeta_{\epsilon^2\epsilon^3} \equiv \left\langle \boldsymbol{\rho}^1_{\epsilon^2\epsilon^3} 2\mathbf{I}^1_{\mathsf{z}} \right\rangle$ be the y and z components of the data spin's constituent density matrices ($\epsilon^2, \epsilon^3 \in \{\pm 1\}$), one can show that in this case the matrix derivative at $t = 0$ vanishes if and only if

$$\begin{aligned} \dot{\Theta}_{++}\upsilon_{++} + \dot{\Theta}_{+-}\upsilon_{+-} + \dot{\Theta}_{-+}\upsilon_{-+} + \dot{\Theta}_{--}\upsilon_{--} &= 0 \\ \dot{\Theta}_{++}\zeta_{++} + \dot{\Theta}_{+-}\zeta_{+-} + \dot{\Theta}_{-+}\zeta_{-+} + \dot{\Theta}_{--}\zeta_{--} &= 0 \end{aligned} \tag{72}$$

where the $\Theta_{\epsilon^2\epsilon^3}$ are obtained by changing the signs of F^2 and F^3 in our expression for $\Theta \equiv \Theta_{++}$. Since $\dot{\Theta}_{++}(0) = 0$, this is a system of two linear equations in the three unknowns $-2\dot{F}^1 = c^{11}$, $-2\dot{F}^2 = c^{22}$ and $-2\dot{F}^3 = c^{33}$, which is generally solvable. Nevertheless, the coefficients in these equations depend on the state of the data to be protected and its correlations with the ancillae, which makes it impossible to use the three-bit code to protect unknown data in this case.

Figure Captions

1. Diagram giving an overview of the error correction procedure. The three spins correspond to the three horizontal lines. Vertical lines connecting them are quantum gates (unitary operations), where "x" indicates a target spin and "●" a control spin. The first dashed box is the encoding step, which consists of two successive c-NOT's (see text). The filled box with the lightning bolt indicates decoherence through random rotations about the x-axis. The second dashed box is the decoding step, while the third is the Toffoli gate which corrects for decoherence to first order. The final filled triangle and square indicates that the ancillae are decoupled while the data spin is observed.

2. RF and gradient pulse sequence diagrams to implement both the totally correlated (a) and uncorrelated (b) decoherence models. In the figure, black boxes indicate $(\pi)^{12}$ RF pulses, and grey boxes indicate $(\pi)^{13}$ pulses, while the graph on the G_z line indicates the gradient polarity. The remaining symbols are defined in the main text.

3. Plots showing the experimental results for quantum error correction applied to the $\mathbf{I}_z^1\mathbf{E}_+^2\mathbf{E}_+^3$ state (cf. Figure **??**). The "decoherence time" is the time allowed for diffusion in the gradient-diffusion procedure (see text). The amplitudes are of the peak due to the data spin, following a $\pi/2$ readout pulse, relative to its amplitude with no decoherence. The "x" symbols mark the amplitudes of the peak following the error correction procedure at 32 equally spaced decoherence times. The "+" symbols mark the amplitudes of the peak as a function of the decoherence time when the gradient-diffusion procedure was applied to the $\mathbf{I}_x^1$ state with no error correction at the same 32 time points. These measurements were averaged over 16 repetitions of each experiment (without any phase cycling). The rate of decay of the peak $1/\tau = 2.5677\ \mathrm{sec}^{-1}$ due to decoherence was obtained by a linear least-squares fit to the logarithm of the amplitudes of the peak from the $\mathbf{I}_x^1$ state (lower curve, correlation coefficient -0.9987), after which the decay with error correction was obtained from the theoretical relation $(9\exp(-t/\tau) - \exp(-9t/\tau))/8$ (upper curve, correlation coefficient 0.9873).

4. Plots showing the experimental results for quantum error correction applied to the $\mathbf{I}_y^1\mathbf{E}_+^2\mathbf{E}_+^3$ state. As in Figure **??**, the "x" symbols mark the amplitudes of the peak due to the

data spin at 32 equally spaced decoherence times (note that the amplitudes at $t = 0.0145$ and $t = 0.1265$ sec were treated as outlyers and omitted), averaged over 16 repetitions of each experiment. The "+" symbols mark the amplitudes of the peak from the $\mathbf{I}_{\mathsf{y}}^1$ state with no error correction, averaged over 8 repetitions of each experiment. The rate of decay of the peak $1/\tau = 2.4200\ \mathrm{sec}^{-1}$ due to decoherence was obtained by a linear least-squares fit to the logarithm of the amplitudes of the peak from the $\mathbf{I}_{\mathsf{y}}^1$ state (lower curve, correlation coefficient -0.9962), after which the decay with error correction was predicted from the theoretical relation $(9\exp(-t/\tau) - \exp(-9t/\tau))/8$ (upper curve, correlation coefficient 0.9867).

5. Plots showing the experimental results for quantum error correction applied to the $\mathbf{I}_{\mathsf{x}}^1\mathbf{E}_+^2\mathbf{E}_+^3$ state. As in Figure **??**, the "x" symbols mark the amplitudes of the peak due to the data spin at 16 equally spaced decoherence times, averaged over 32 repetitions of each experiment. The decay rate of the peak $1/\tau = 0.2084$ due to decoherence was obtained by a linear least-squares fit to the logarithm of the amplitudes of the peak (solid line, correlation coefficient -0.6022), indicating that it is not decohered by gradient-diffusion nor otherwise affected by the error correction procedure.

6. Plots showing the experimental results for quantum error correction applied to the $\mathbf{I}_{\mathsf{z}}^1\mathbf{E}_+^2\mathbf{E}_+^3$ state, with independent gradient-induced decoherence for each spin. As in Figure **??**, the "x" symbols mark the amplitudes of the peak due to the data spin at 32 equally spaced decoherence times averaged over 16 repetitions of each experiment. The "+" symbols mark the amplitudes of the peak from the $\mathbf{I}_{\mathsf{x}}^1\mathbf{E}_+^2\mathbf{E}_+^3$ state without encoding, decoding or error correction, averaged over 16 repetitions of each experiment. The rate of decay of the peak $1/\tau = 3.2931\ \mathrm{sec}^{-1}$ due to decoherence was obtained by a linear least-squares fit to the logarithm of the amplitudes of the peak from the data spin as a function of decoherence time (lower curve, correlation coefficient -0.9970), after which the decay with error correction was predicted from the theoretical relation $(3\exp(-t/\tau) - \exp(-3t/\tau))/2$ (upper curve, correlation coefficient 0.9546). The decay curve predicted for totally correlated decoherence as in Figure **??** is shown with a dashed line for comparison.

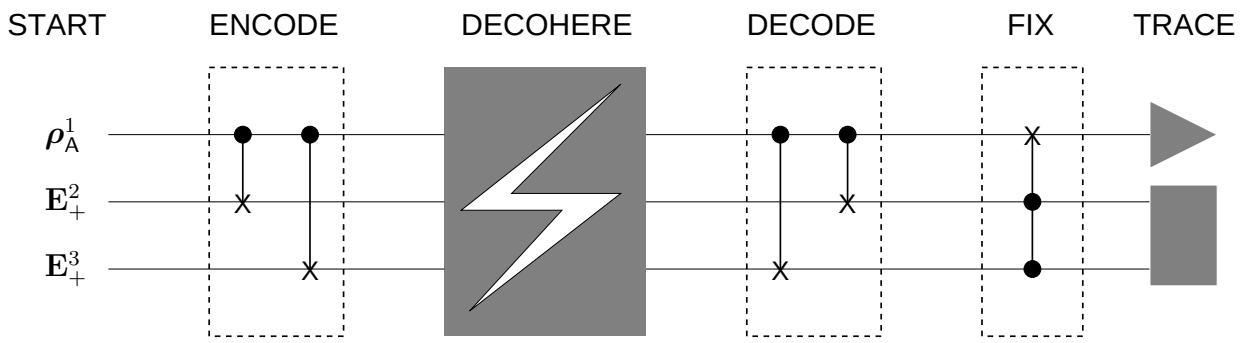
START
ENCODE
DECOHERE
DECODE
FIX
TRACE
ρ_{A}^{1}
$\mathbf{E}_{+}^{2}$
$\mathbf{E}_{+}^{3}$

Figure 1.

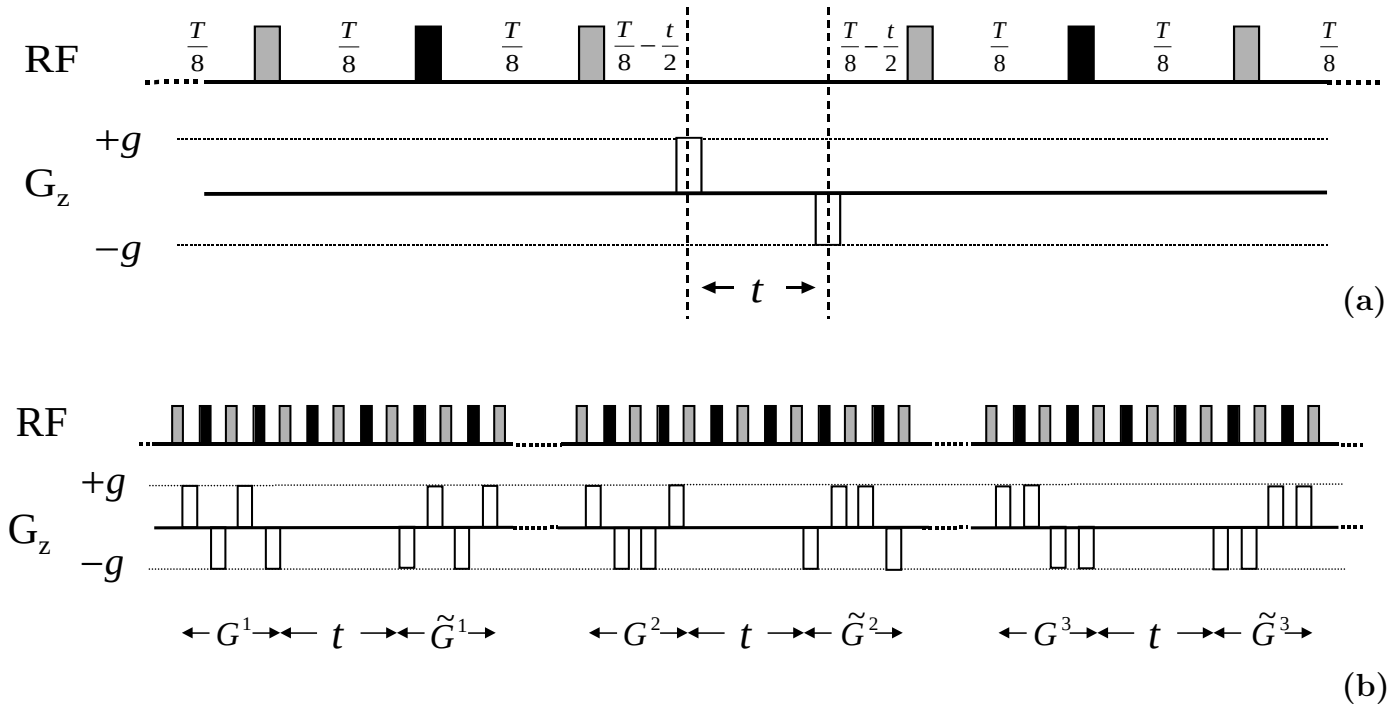
RF
$\frac{T}{8}$
$\frac{T}{8}$
$\frac{T}{8}$
$\frac{T}{8}-\frac{t}{2}$
$\frac{T}{8}-\frac{t}{2}$
$\frac{T}{8}$
$\frac{T}{8}$
$\frac{T}{8}$
$+g$
G_z
$-g$
t
(a)
RF
$+g$
G_z
$-g$
G^1 t $\tilde{G}^1$
G^2 t $\tilde{G}^2$
G^3 t $\tilde{G}^3$
(b)

Figure 2.

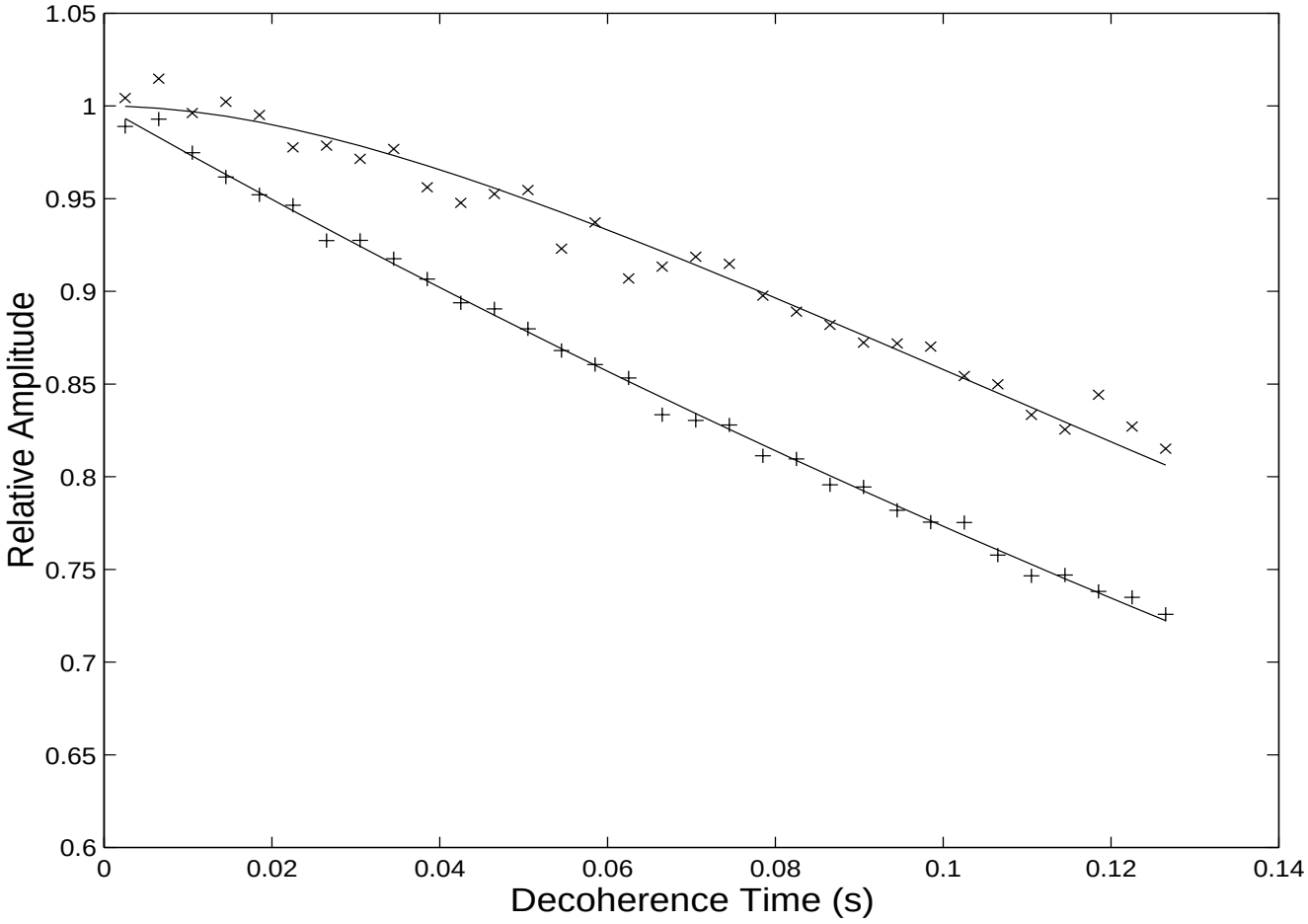
1.05
1
0.95
0.9
0.85
0.8
0.75
0.7
0.65
0.6
Relative Amplitude
0
0.02
0.04
0.06
0.08
0.1
0.12
0.14
Decoherence Time (s)

Figure 3.

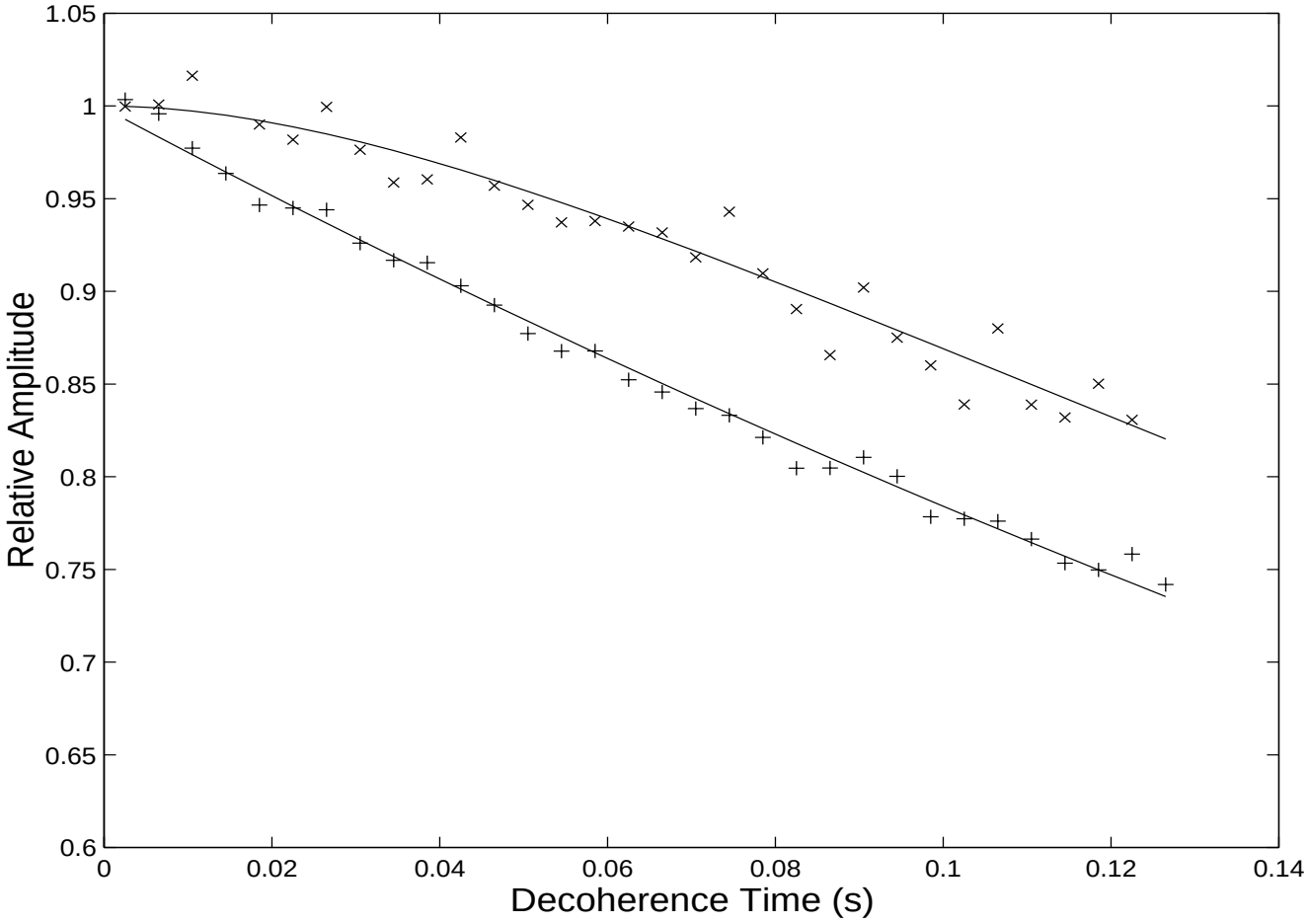
1.05
1
0.95
0.9
0.85
0.8
0.75
0.7
0.65
0.6
Relative Amplitude
0
0.02
0.04
0.06
0.08
0.1
0.12
0.14
Decoherence Time (s)

Figure 4.

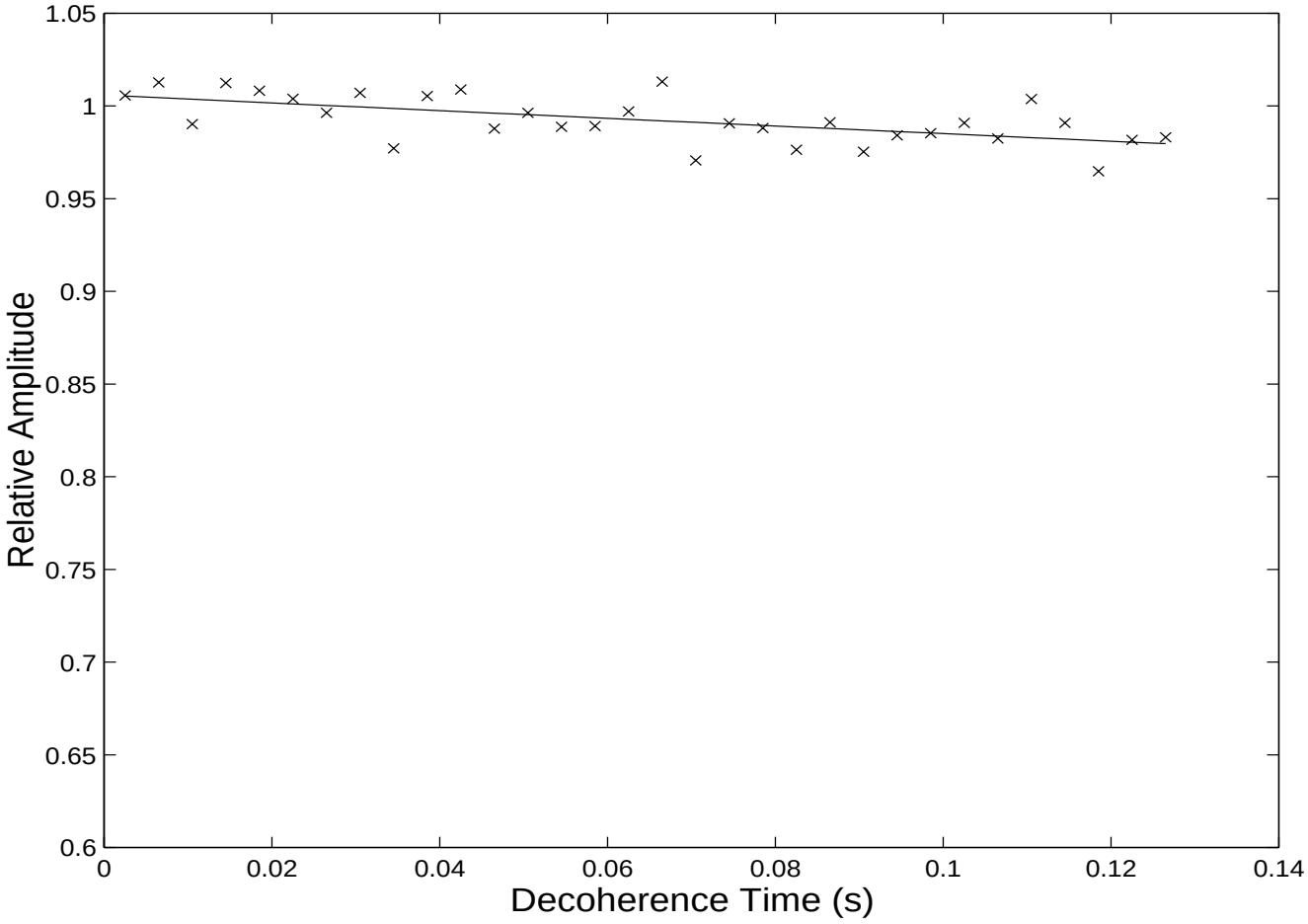
1.05
1
0.95
0.9
0.85
0.8
0.75
0.7
0.65
0.6
Relative Amplitude
0
0.02
0.04
0.06
0.08
0.1
0.12
0.14
Decoherence Time (s)

Figure 5.

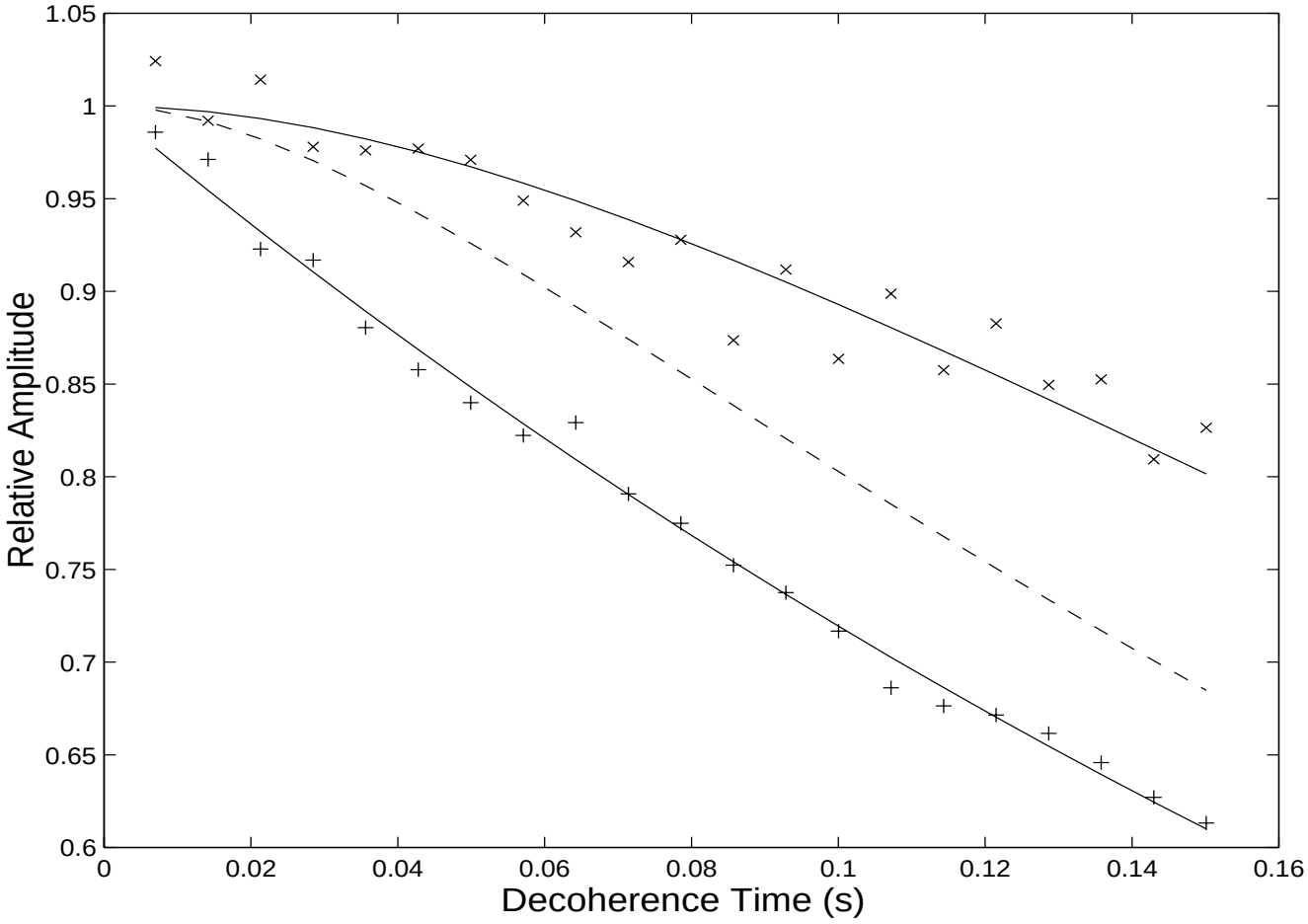
1.05
1
0.95
0.9
0.85
0.8
0.75
0.7
0.65
0.6
Relative Amplitude
0
0.02
0.04
0.06
0.08
0.1
0.12
0.14
0.16
Decoherence Time (s)

Figure 6.